Hydrol. Earth Syst. Sci., 30, 3741–3762, 2026
https://doi.org/10.5194/hess-30-3741-2026


Hydrology and Earth System Sciences
Open Access
EGU

# A coupled surface water-groundwater multi-objective optimization framework for coordinated water-ecosystem-agriculture management in arid inland river basin

**Danhong Chen**[1], **Xiankui Zeng**[1], **Dongwei Gui**[2], **Dong Wang**[1], **and Jichun Wu**[1]

[1]Key Laboratory of Surficial Geochemistry, Ministry of Education, School of Earth Sciences and Engineering, Nanjing University, Nanjing, China
[2]Cele National Station of Observation and Research for Desert-Grassland Ecosystem, Xinjiang Institute of Ecology and Geography, Chinese Academy of Sciences, Urumqi, China

**Correspondence:** Xiankui Zeng (xiankuizeng@nju.edu.cn)

Received: 5 January 2026 – Discussion started: 15 January 2026
Revised: 8 April 2026 – Accepted: 4 June 2026 – Published: 22 June 2026

**Abstract.** In arid regions, water is the key link sustaining both production and ecosystems, and its sustainable management is essential for regional security. This study constructs a coupled surface water-groundwater hydrology-agriculture multi-objective optimization model for the mainstream area of the Tarim River Basin, in which the NSGA-III algorithm is applied to optimize four objectives, including agricultural economic benefit per unit of irrigation water ($f_{\mathrm{AB}}$), groundwater level rise ($f_{\mathrm{GL}}$), terminal lake area ($f_{L_A}$), and total agricultural nitrogen load ($f_{\mathrm{TN}}$). Based on the optimized solutions, the trade-offs and synergistic pathways among multiple objectives within the water-ecosystem-agriculture system are systematically evaluated under different hydrological year conditions. The results indicate that significant trade-offs exist among objectives, with $f_{\mathrm{AB}}$ showing negative relationships with $f_{\mathrm{TN}}$ and $f_{L_A}$, and solutions with higher economic benefits generally accompanied by reduced ecological water supply and increased nitrogen loads. The spatial heterogeneity of the basin necessitates the adoption of differentiated management strategies, whereby upstream areas with relatively stable water availability can sustain higher levels of agricultural production, while midstream and downstream areas are highly sensitive to ecological water constraints and therefore require priority allocation to ecological water use. The optimization results show that cultivated land area should be dynamically adjusted under different hydrological conditions, ranging from $11.3 \times 104$–$14.3 \times 104\,\mathrm{hm}^2$ in wet years, $10.1 \times 104$–$13.1 \times 104\,\mathrm{hm}^2$ in normal years, and contracting to $9.5 \times 104$–$11.9 \times 104\,\mathrm{hm}^2$ in dry years. The cropping structure is dominated by cotton (69.7 %–75.8 %), with the proportion of high-benefit crops such as vegetables and fruit crops moderately increased in wet years, whereas in dry years the structure shifts toward water-saving crops and high water-consuming crops are appropriately restricted. This study demonstrates that combining multi-objective optimization with spatially differentiated regulation can achieve coordinated management of water resources, ecosystems, and agriculture, and provides an operational decision-making basis for managing water-ecosystem-agriculture systems in arid inland river basins.

## 1 Introduction

The continuous growth of the global population and the expansion of cultivated areas have exacerbated the imbalance between water availability and demand, with particularly severe impacts in arid and semi-arid regions (IPCC, 2022; Flörke et al., 2018; Cosgrove and Loucks, 2015; Watson et al., 2013). Agriculture is responsible for nearly 70 % of global freshwater withdrawals (FAO, 2012) and contributes nearly 25 % of global greenhouse gas emissions (Campbell et al., 2017). Under the combined pressures of water scarcity and ecosystem vulnerability, improving the understanding of interactions within the water-ecosystem-agriculture (WEA) system and developing coordinated multi-objective opti-

mization frameworks have become critical for achieving sustainable water resources management (Yin et al., 2022; Song et al., 2020; Jalilov et al., 2018; Avellán et al., 2018).

In recent years, multi-objective simulation optimization (S-O) frameworks have been increasingly applied to basin-scale water resources management and planning. By coupling process-based simulation models with multi-objective optimization algorithms, these frameworks provide an effective means of exploring trade-offs among water allocation, ecosystem protection, and agricultural production within the WEA system (Song et al., 2020; Niu et al., 2019; Karner et al., 2021; Wang et al., 2022; Cao et al., 2023; Naranjo et al., 2023). For instance, Niu et al. (2019) employed a multi-objective linear fractional programming model to assess the interactions and trade-offs among water resources, ecosystems, and agriculture activities in the Zhangye Basin. Yin et al. (2022) coupled a SEAWAT-RT3D model with multi-objective optimization to quantify trade-offs between agricultural net benefits, seawater intrusion, and nitrate contamination in the Dagu River Basin. Similarly, Zhang and Ren (2021) and Tang et al. (2024) applied S-O frameworks in the Haihe River Basin and the Yanqi Basin, respectively, and achieved coordinated improvements in economic and ecological outcomes under regulated water allocation scenarios. These studies demonstrate the applicability and effectiveness of S-O frameworks for addressing WEA trade-offs at the regional scale.

The mainstream reach of the Tarim River Basin represents a representative arid inland river system in China (Wang et al., 2020). Agricultural production in this region is highly dependent on hydraulic infrastructure and is characterized by intensive irrigated agriculture (Hartmann et al., 2016). Long-term and large-scale abstraction of groundwater and diversion of surface water for irrigation have supported regional agricultural development and food security. However, these practices have also resulted in pronounced ecosystem degradation, manifested by declining groundwater levels, intensified desertification, and the shrinkage of terminal lakes (Lu et al., 2026; Zhang et al., 2013; Pang et al., 2010). Consequently, the need to balance agricultural water use with ecosystem stability has become a critical concern for the oversight of water resources in the Tarim River Basin.

In response to these challenges, numerous studies have investigated agricultural irrigation efficiency, ecological water allocation, and optimal water resources management in the basin. Chen (2019) developed a bi-objective optimization model to analyze benefit allocation between agricultural and ecological water uses under different inflow scenarios. Jia (2020) proposed an ecological water-use priority system and ecological replenishment strategies based on eco-gate control zones. Zhu (2022) established a regional water allocation optimization model to support the coordinated operation of multiple water sources. From a water-energy-food (WEF) nexus perspective, Feng et al. (2022) assessed the irrigation requirements and overall efficiency of resource utilization for the main crops in the basin.

Despite these advances, the existing studies still exhibit limitations in their representation of the physical mechanisms and coordinated management of the WEA system. These studies often rely on simplified modeling approaches that treat surface water and groundwater as separate components, thereby failing to capture their dynamic interactions. This limitation constrains the accurate quantification of the impacts of land-use change or cropping structure adjustment on groundwater dynamics and ecosystem responses. In addition, ecological water requirements are often represented as fixed minimum thresholds, which overlook the dynamic regulatory role of surface water-groundwater interactions over time. As a result, ecological constraints are not effectively incorporated into optimization-based decision-making processes. Moreover, most existing studies focus on single or dual objectives, such as agriculture-ecology or agriculture-economy, and lack a comprehensive optimization framework that systematically characterizes trade-offs among water resources, ecosystems, and agriculture within the WEA system.

To address these limitations, this study develops a WEA collaborative optimization framework for the mainstream reach of the Tarim River Basin by integrating a coupled surface water-groundwater model, multi-objective optimization, and dynamic ecological constraints. The objectives of this study are twofold. First, a multi-objective S-O model incorporating surface water-groundwater interactions is constructed to achieve coordinated optimization of water resources, ecosystems, and agriculture within the WEA system of the Tarim River mainstream region. Second, based on the proposed WEA optimization framework, critical thresholds of cultivated land expansion and optimal cropping structures under different hydrological conditions are identified. This study aims to provide scientific support for sustainable water resources management in arid inland river basins.

The remainder of this paper is organized as follows. Section 2 describes the study area and data sources. Section 3 details the adopted modeling approach, covering the coupled surface water-groundwater simulation, the multi-objective optimization method, and the evaluation metrics. Section 4 reports the simulation and optimization results. Section 5 provides a discussion of the results and their implications, while Section 6 summarizes the main conclusions and outlines future research directions.

## 2 Study area and data

### 2.1 Study area

The mainstream region of the Tarim River Basin is situated in northern Xinjiang, China, between the southern alluvial plain of the Tianshan Mountains and the northern margin of

the Taklimakan Desert. The study region stretches westward from the Alar region, where the Aksu, Yarkant, and Hotan rivers merge, eastward to the terminal Taitema Lake (Fig. 1). The study area covers approximately 40 956 $km^2$, featuring a gently eastward-sloping topography with elevations ranging from 805 to 1023 m.

The region exhibits a temperate continental arid climate, characterized by an annual mean temperature of 10.6 °C and total precipitation below 80 mm, mainly occurring from May to August, while the annual potential evapotranspiration is over 2500 mm (Tuoliewubieke et al., 2025; Cui et al., 2024; Ling et al., 2014). Water resources primarily originate from mountain glacier/snowmelt and upstream inflow diversions, exhibiting the arid-region characteristics of source-dominated supply with high spatiotemporal variability (Grashey-Jansen et al., 2014).

The Tarim River mainstream stretches approximately 1321 km in a west-east direction and is typically categorized into upstream, midstream, and downstream sections (Cui et al., 2024; Chen et al., 2006). The river exhibits a strongly seasonal flow pattern, with 70 %–85 % of the annual runoff occurring from June and September. Peak flows usually occur in July or August, whereas minimum flows are typically recorded in January and February. Surface water and groundwater systems within the region are closely connected, with frequent interactions influencing regional water availability.

Agriculture is the dominant economic activity in the Tarim River mainstream region. By 2015, approximately 1307 $km^2$ of land were under irrigation, of which about 1073 $km^2$ is cultivated land (Xinjiang Uygur Autonomous Region Bureau of Statistics, 2016). Major crops include cotton, maize, vegetables, and fruits. Since 1990, the cultivated land area has expanded by over 60 %, with oasis farmland continually encroaching into desert margins.

The area contains several large irrigation districts, where water for irrigation is primarily drawn from the Tarim River mainstream, supplemented by groundwater (Hao et al., 2015). Considerable differences in management and irrigation efficiency among these districts have placed significant pressure on the distribution of mainstream water resources, complicating regional water management.

The downstream ecosystem is extremely fragile. Ecological degradation has intensified since the 1950s with the area of Populus euphratica forests decreasing by approximately 86 % compared to historical conditions (Jiang et al., 2005). The river reaches between Daxihaizi Reservoir and Taitema Lake experienced prolonged channel desiccation, including a continuous dry-up of nearly 400 km at its most severe stage. As a result, Taitema Lake remained dry for extended periods, and the margins of the Taklimakan and Kuruk deserts approached near connection.

To mitigate ecological degradation in downstream reaches, China launched the Ecological Water Conveyance Project (EWCP) along the Tarim River mainstream in 2000, aiming to restore river connectivity, groundwater levels, and riparian vegetation in downstream areas (Gao et al., 2026; Wang et al., 2025; Jiao et al., 2022; Dou et al., 2022; Xu et al., 2007). According to recent monitoring and official reports, 26 ecological water conveyance events had been conducted by 2025, delivering a cumulative volume of approximately 10.2 billion $m^3$.

The ecological water conveyance has substantially improved riparian vegetation coverage, wetland area, and groundwater levels along the downstream river corridor, playing a critical role in the recovery of ecosystem functions (Liao et al., 2020).

Despite these improvements, continued agricultural expansion upstream has increased diversion demands, while interannual inflow variability further strains ecological water regulation. Consequently, there remains a need to further optimize mainstream water resources allocation, improve irrigation water use efficiency, and achieve a dynamic balance between ecological water conveyance and agricultural development, in order to safeguard basin-wide ecological security and socio-economic sustainability.

### 2.2 Data

The datasets used in this research encompass topography, land use, climate, hydrogeology, and socio-economic information, with a primary temporal coverage from 2002 to 2021.

Snow cover information was obtained from the High Asia MODIS daily snow cover fraction product developed by Qiu and Wang (2020). This dataset, derived using the MODIS Normalized Difference Snow Index (NDSI), offers daily data at a spatial resolution of 500 m and serves as a critical input for the snowmelt runoff model (SRM). Terrain-related information was sourced from the Advanced Spaceborne Thermal Emission and Reflection Radiometer Global Digital Elevation Model (ASTER GDEM), which has a spatial resolution of 30 m (NASA/METI/AIST/Japan Spacesystems and U.S./Japan ASTER Science Team, 2019). These elevation data were used to extract terrain attributes, including slope, aspect, and river networks.

Land use, vegetation, and soil property data were obtained from multiple sources. Land cover information was obtained from the FROM-GLC dataset (Gong et al., 2013), soil properties were derived from the Harmonized World Soil Database (Wieder et al., 2014), and vegetation attributes were derived from the Vegetation Map of China (Hou et al., 2019). Collectively, these datasets provided key inputs for simulating land surface processes and parameterizing soil-related processes in the coupled model.

Hydrogeological conditions were primarily derived from borehole data and regional hydrogeological maps reported by Li et al. (2003). Key parameters, including hydraulic conductivity and specific yield, were assigned based on dominant lithological units.

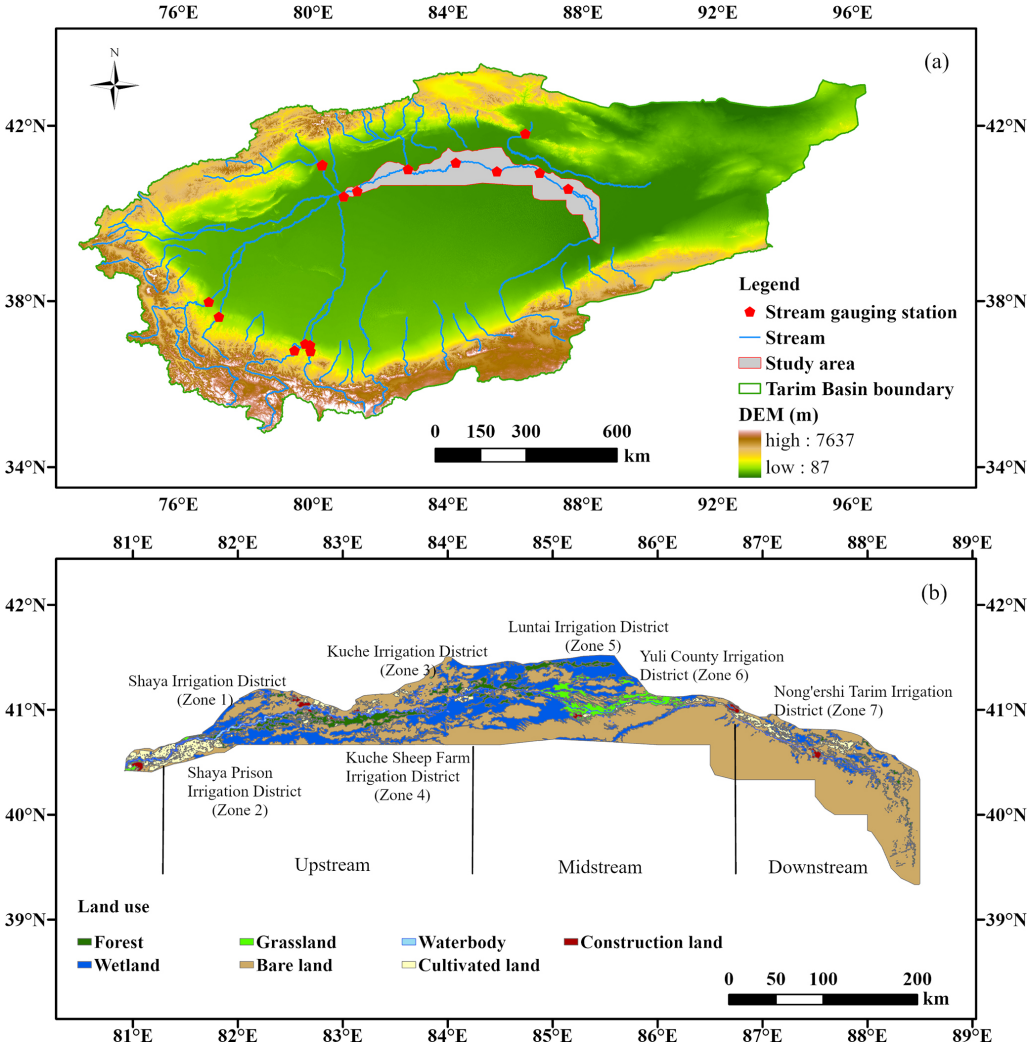


**Figure 1. (a)** The location of the Tarim River mainstream region. **(b)** Land use types across the Tarim River mainstream region. Sources: Esri | Powered by Esri; Basemap: Esri World 286 Hillshade (Esri).

Meteorological forcing for the coupled surface water-groundwater model consisted of precipitation and temperature (maximum and minimum), which were obtained from the ERA5 reanalysis dataset (Hersbach et al., 2020). Model calibration and validation for the groundwater component relied on monthly groundwater level measurements from 139 monitoring wells distributed throughout the study area (Xue et al., 2024).

Daily streamflow records from five representative hydrological stations within the Tarim River Basin (2002–2021) were used to calibrate surface runoff simulations and model parameters.

To further evaluate the groundwater simulations of the GSFLOW model, terrestrial water storage anomaly (TWSA) data from the GRACE and GRACE-FO satellite missions (Save et al., 2016; Save, 2020) were used for model validation. In addition, the coupled model was cross-validated using evapotranspiration (GLEAM) (Martens et al., 2017) and soil moisture (Chinese Soil Moisture Dataset) (Meng et al., 2021a, b). A comprehensive summary of all datasets employed in this study is provided in Table S1.

Socio-economic data were primarily collected from the China Statistical Yearbook (National Bureau of Statistics of China, 2021), Xinjiang Water Resources Bulletin (Xinjiang Uygur Autonomous Region Water Resources Department, 2021), and the National Agricultural Product Cost-Benefit Compilation together with annual crop price statistics (Ministry of Agriculture and Rural Affairs of Xinjiang, 2025). These datasets provide information on crop planting areas, yields, and fertilizer and pesticide application rates.

## 3 Methodology

This study develops a comprehensive decision-oriented framework that combines a coupled surface water-groundwater simulation with a multi-objective optimization approach. The framework is designed to simulate hydrological processes within the Tarim River mainstream region and to achieve coordinated optimization of agricultural and ecological water demands under limited water availability. The overall modeling system consists of three components. The first component is a GSFLOW-based hydrological model that simulates interactions between surface water and groundwater. The second component is a snowmelt runoff model (SRM), which captures snow and glacier melt processes occurring in the mountainous headwater areas of the basin. The third component is a multi-objective water-ecosystem-agriculture (WEA) optimization model, which is applied to coordinate water allocation among water resources, ecosystems, and agricultural production. The overall framework of this study is illustrated in Fig. 2.

### 3.1 Coupled hydrological simulation

Although the primary focus of this study is the Tarim River mainstream region, accurate representation of surface water-groundwater exchanges necessitates hydrological simulations at the scale of the entire Tarim River Basin. The hydrological simulation framework consists of the SRM and the GSFLOW model. The SRM is applied to simulate snow and glacier melt runoff at the mountain outlets, and the simulated results are subsequently used as the upstream inflow boundary for the GSFLOW model. GSFLOW model is then employed to simulate hydrological processes across the Tarim River plain and downstream desert areas. The basin-scale simulation outputs are then used to extract boundary conditions and fluxes for the mainstream region, which serves as the domain for the subsequent multi-objective WEA optimization.

#### 3.1.1 Coupled surface water-groundwater model

The coupled surface water-groundwater model is developed based on the GSFLOW framework proposed by Chen et al. (2025), with model parameters recalibrated in this study. GSFLOW is a physically based distributed coupled hydrological modeling system that integrates the PRMS (Precipitation-Runoff Modeling System) surface hydrological process module with the MODFLOW groundwater flow module to simulate surface water-groundwater interactions at the watershed scale (Markstrom et al., 2008). The model is capable of simulating key hydrological processes such as precipitation, evapotranspiration, infiltration, surface runoff, groundwater recharge, and stream-aquifer exchange. Specifically, we incorporated additional streamflow observations from three mainstream stations (Yingbazha, Usman, and Qiala) to refine parameter estimation. Diversion flows from major mainstream irrigation canals were also adjusted during calibration.

The modeling domain encompasses the Tarim River plain and surrounding desert areas and is discretized at a spatial resolution of 2 km × 2 km, yielding a total of 212 928 hydrologic response units (HRUs). The groundwater system is discretized into six layers, comprising 692 658 active grid cells.

Surface processes (infiltration, evapotranspiration, irrigation recharge) are parameterized based on geomorphology, land use, and crop distribution. Irrigation infiltration and groundwater abstraction volumes are derived from the Xinjiang Water Resources Bulletin (2002–2021). Other key parameters (e.g., infiltration coefficients, aquifer hydraulic conductivity) were calibrated using a Bayesian uncertainty analysis framework.

The simulation period spans 2002–2021, with 2002–2006 designated as the warm-up period, 2007–2016 as the calibration period, and 2017–2021 as the validation period. Model calibration and validation are conducted using observed groundwater levels and streamflow data from major hydrological stations. Additional evaluation of the calibrated GSFLOW model is conducted using GRACE-based terrestrial water storage change (TWSC), evapotranspiration data from the GLEAM product, and soil moisture data from the SMC dataset.

Model performance is quantified using the Nash-Sutcliffe efficiency (NSE) and the coefficient of determination ($R^2$), defined as follows:

$$\mathrm{NSE} = 1 - \frac{\sum_{i=1}^{n}\left(Q_{\mathrm{sim}}(i) - Q_{\mathrm{obs}}(i)\right)^2}{\sum_{i=1}^{n}\left(Q_{\mathrm{obs}}(i) - \overline{Q}_{\mathrm{obs}}\right)^2} \tag{1}$$

$$R^2 = \frac{\left[\sum_{i=1}^{n}\left(Q_{\mathrm{obs}}(i) - Q_{\mathrm{obs}}(i)\right)\left(Q_{\mathrm{sim}}(i) - \overline{Q}_{\mathrm{sim}}(i)\right)\right]^2}{\left[\sum_{i=1}^{n}\left(Q_{\mathrm{obs}}(i) - \overline{Q}_{\mathrm{obs}}\right)^2\right]\left[\sum_{i=1}^{n}\left(Q_{\mathrm{sim}}(i) - \overline{Q}_{\mathrm{sim}}\right)^2\right]} \tag{2}$$

where $n$ is the length of the observation series; $Q_{\mathrm{obs}}(i)$ and $Q_{\mathrm{sim}}(i)$ denote the observed and simulated values at time step $i$, respectively; and $Q_{\mathrm{obs}}$ and $Q_{\mathrm{sim}}$ represent their corresponding mean values. Both NSE and $R^2$ range from 0 to 1, with values approaching 1 indicating stronger agreement between simulations and observations.

#### 3.1.2 Snowmelt runoff model (SRM)

Snow and glacier melt from mountainous regions represent a critical source of water supply in the Tarim River Basin. To account for these processes, the SRM model is applied to simulate daily snowmelt runoff. The model incorporates temperature, precipitation, and snow cover fraction, and is expressed as follows:

$$Q_{n+1} = \left[c_{\mathrm{sn}} \cdot M_n \cdot S_n + c_{\mathrm{Rn}} \cdot P_n\right] \cdot A \cdot \frac{10\,000}{86\,400}(1 - k_{n+1}) + Q_n \cdot k_{n+1} \tag{3}$$

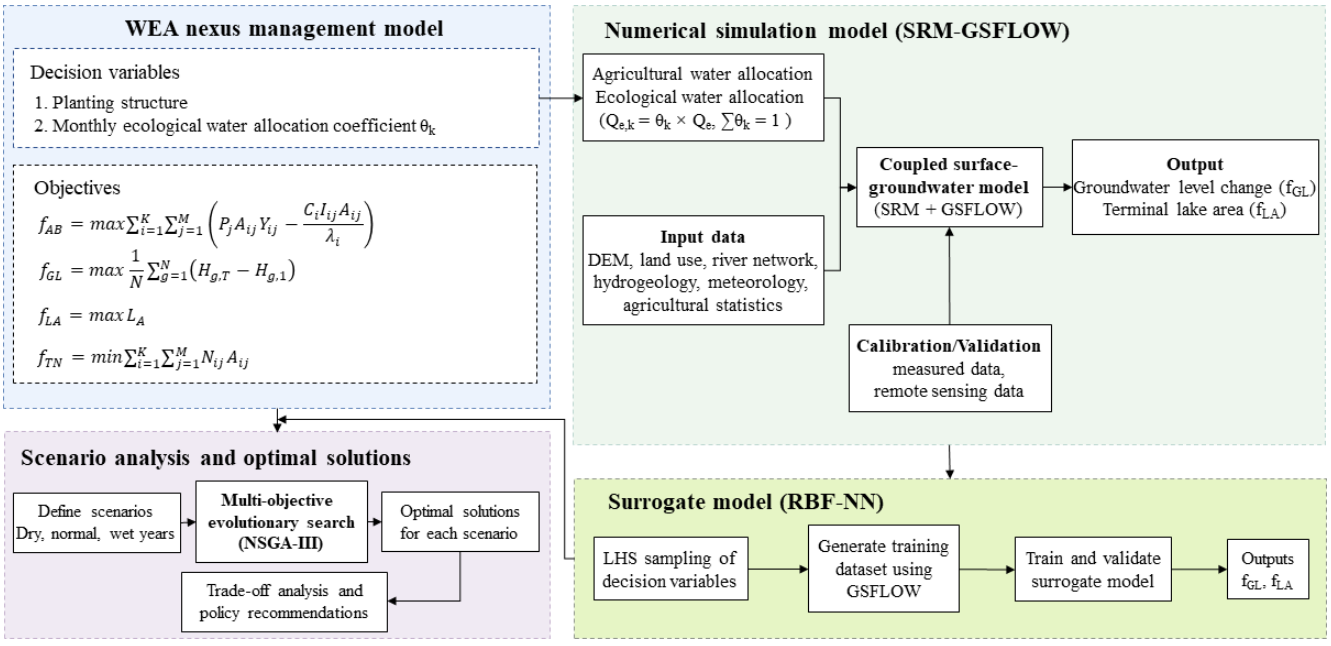


**Figure 2.** Framework of the multi-objective simulation – optimization for the WEA nexus management.

where $Q_{n+1}$ is the mean daily discharge on day $n+1$ ($m^3\ s^{-1}$); $M_n$ and $P_n$ are the snowmelt depth ($cm\ d^{-1}$) and precipitation (cm) on day $n$, respectively; $S_n$ is the snow cover fraction; $c_{sn}$ and $c_{Rn}$ are the runoff coefficients for snowmelt and rainfall; $A$ is the basin area ($km^2$); $k_{n+1}$ is the recession coefficient representing runoff decay under no recharge conditions; and the factor 10 000/86 400 converts runoff depth (cm) to discharge ($m^3\ s^{-1}$).

## 3.2 Multi-objective optimization model

To promote the coordinated development of agricultural production, ecosystem protection, and sustainable water resources use, a multi-objective water-ecosystem-agriculture (WEA) optimization model was developed for the Tarim River Basin mainstream region. Based on regional geomorphological features and hydrological conditions, the mainstream area was initially categorized into three major sections: upstream, middle, and downstream reaches. Each section was further partitioned into seven agricultural management sub-units. This zoning scheme primarily follows administrative divisions in combination with the spatial distribution of major irrigation districts. The seven agricultural sub-units include the Shaya Irrigation District (Zone 1), Shaya Prison Irrigation District (Zone 2), Kuqa Irrigation District (Zone 3), Kuqa Sheep Breeding Farm Irrigation District (Zone 4), Luntai Irrigation District (Zone 5), Yuli County Irrigation District (Zone 6), and the Second Agricultural Division Tarim Irrigation District (Zone 7). The geographical arrangement of these sub-units is illustrated in Fig. 1b.

### 3.2.1 Decision variables

The proposed multi-objective optimization model includes two categories of decision variables, namely crop planting areas and monthly ecological water allocation coefficients.

1. Crop planting area ($A_{ij}$)

   For model implementation, the mainstream region is divided into multiple agricultural zones according to natural geographic attributes and administrative boundaries. Within each zone, multiple crop types are considered, including maize, cotton, vegetables, melons, fruit trees, and oilseeds. The variable $A_{ij}$ denotes the cultivated area of crop $j$ in agricultural zone $i$, expressed in units of thousand hectares.

2. Monthly ecological water allocation coefficient ($\theta_k$)

   To represent the seasonal characteristics of ecological water demand, the period from May to September is identified as the key ecological water replenishment period. The coefficient $\theta_k$ represents the proportion of the annual total ecological water allocation assigned to month $k$. During the hydrological model coupling process, the monthly ecological water conveyance is introduced into the GSFLOW model as an additional river diversion boundary condition and simulated through the SFR module in MODFLOW. After entering the river system, the ecological water first changes river discharge and river stage, and then affects groundwater recharge through riverbed leakage mechanisms. When the river stage is higher than the groundwater level, the

river recharges the aquifer; otherwise, groundwater may discharge to the river. Therefore, the monthly ecological allocation coefficient $\theta_k$ becomes an important variable linking the multi-objective optimization decisions with hydrological process simulations.

#### 3.2.2 Constraints

To ensure that the optimization process complies with regional hydrological conditions and ecological safety requirements, the following constraints are imposed.

1. Groundwater depth constraint

   The groundwater depth in each ecological zone is required to remain within a suitable range for vegetation growth and sustainability. This constraint is expressed as:

   $$D_{\min} \leq D_{s,t} \leq D_{\max} \tag{4}$$

   where $D_{s,t}$ denotes the groundwater depth in zone $s$ at time $t$. Based on previous studies, the suitable groundwater depth ranges are 3–6 m for forestland, 2–5 m for grassland, and 4.5–7 m for desert vegetation (Wang et al., 2020).

2. Terminal lake area constraint

   The surface extent of Taitema Lake, as the terminal lake, is constrained to remain within a prescribed range in order to maintain its basic ecological functions. The constraint is defined as:

   $$L_{A_{\min}} \leq L_A \leq L_{A_{\max}} \tag{5}$$

   where $L_{A_{\min}}$ and $L_{A_{\max}}$ are set to 30 and 110 $\mathrm{km}^2$, respectively. These values are derived from remote sensing observations over the past 30 years and studies on ecological water requirements, which indicate that this range is sufficient to sustain key ecosystem functions and biodiversity within the lake system (Ye et al., 2022; Wang et al., 2021).

3. Canal conveyance capacity constraint

   The diversion flows allocated to agricultural and ecological zones must not exceed the conveyance capacity of the canal system. This constraint is formulated as:

   $$Q_{a,i} \leq Q_{\max,i} \tag{6}$$
   $$Q_{e,j} \leq Q_{\max,j} \tag{7}$$

   where $Q_{a,i}$ and $Q_{e,j}$ represent the diversion flows for agricultural zone $i$ and ecological zone $j$ ($\mathrm{m}^3$ per month), respectively. The maximum conveyance capacities $Q_{\max}$ are determined based on the design discharge and conveyance capacity of major canals along the mainstream (Wang et al., 2021).

4. Crop water requirement

   The effective irrigation water supplied to each agricultural zone must satisfy the basic water requirements of crops. This requirement is expressed as:

   $$\alpha\beta Q_{a,i} \geq I_{ij} A_{ij} \tag{8}$$

   where $\alpha$ and $\beta$ denote the canal conveyance efficiency and field application efficiency, respectively, and $I_{ij}$ represents the irrigation demand ($\mathrm{m}^3\,\mathrm{hm}^{-2}$) associated with crop $j$ in agricultural zone $i$, $A_{ij}$ denotes the irrigated area of crop j in agricultural zone $i$ ($\mathrm{hm}^2$).

#### 3.2.3 Objective functions

The multi-objective model targets the maximization of agricultural economic benefits, groundwater level recovery, and the surface area of the terminal lake, in parallel with the minimization of total nitrogen load.

1. Maximize agricultural economic benefit per unit of irrigation water

   $$\text{Maximize } f_{\mathrm{AB}} = \frac{\sum_{i=1}^{K}\sum_{j=1}^{M} P_j A_{ij} Y_{ij} - \sum_{i=1}^{K} C_i Q_{a,i}}{\sum_{i=1}^{K} Q_{a,i}} \tag{9}$$

2. Maximize average cumulative groundwater level rise

   $$\text{Maximize } f_{\mathrm{GL}} = \frac{1}{N}\sum_{g=1}^{N} H_{\mathrm{g}}, T - H_{\mathrm{g},1} \tag{10}$$

3. Maximize Taitema Lake surface area

   $$\text{Maximize } f_{L_A} = L_A \tag{11}$$

4. Minimize total nitrogen load

   $$\text{Minimize } f_{\mathrm{TN}} = \sum_{i=1}^{K}\sum_{j=1}^{M} N_{ij} A_{ij} \tag{12}$$

   where $i$ indexes agricultural zones ($i = 1, \ldots, K$, where $K = 7$), and $j$ indexes crop types ($j = 1, \ldots, M$, where $M = 6$, representing maize, cotton, vegetables, melons, fruit trees, and oilseed). $P_j$ represents the unit net economic benefit of crop $j$ (CNY $\mathrm{kg}^{-1}$); $A_{ij}$ denotes the irrigated area of crop $j$ in agricultural zone $i$ ($\mathrm{hm}^2$); $Y_{ij}$ corresponds to the crop yield per unit area ($\mathrm{kg\,hm}^{-2}$); $I_{ij}$ represents the net irrigation quota ($\mathrm{m}^3\,\mathrm{ha}^{-1}$) of crop $j$ in zone $i$; $C_i$ denotes the unit water cost (CNY $\mathrm{m}^{-3}$) in zone $i$; $T$ indicates the number of stress periods ($T = 365$, d); $g$ indexes groundwater grid cells ($g = 1, \ldots, N$, where $N$ is the total number of grid cells); $H_{\mathrm{g},T}$ and $H_{\mathrm{g},1}$ denote the groundwater heads at groundwater grid cell $g$ at the last and first stress periods, respectively; $A_{\mathrm{area}}$ represents the surface area of Taitema Lake

($km^2$); $Q_{a,i}$ and $Q_{e,i}$ denote agricultural and ecological diversion volumes ($m^3$ per month), respectively; and $N_{ij}$ represents the total nitrogen load per unit area of crop $j$ in zone $i$ ($kg\,hm^{-2}$). The crop management parameters are summarized in Table 1.

The above multi-objective optimization problem is addressed using the Non-dominated Sorting Genetic Algorithm III (NSGA-III; Deb and Jain, 2014). This algorithm is particularly effective for handling high-dimensional problems involving multiple objectives and constraints and has been extensively employed in studies of environmental and agricultural resource optimization. The main algorithm parameters are listed in Table 2.

### 3.3 Surrogate model for basin-scale hydrological simulation

Each GSFLOW simulation takes approximately 18 h, presenting a prohibitive computational cost for the simulation-optimization framework. To overcome this, a surrogate model was constructed using a radial basis function neural network (RBF-NN) to represent the relationship between key GSFLOW parameters and the four objective functions in the multi-objective optimization model. The RBF-NN is a multilayer feedforward network with strong nonlinear approximation capability and high computational efficiency. Training samples are generated using Latin hypercube sampling (LHS) to ensure adequate coverage of the parameter space. Following accuracy validation, this surrogate model replaces the original GSFLOW model within the simulation-optimization loop.

To elaborate further, the input variables of the surrogate model are the decision variables to be optimized. Specifically, they include the planting areas of six major crops (cotton, maize, oil crops, vegetables, melons, and fruits) across seven irrigation zones, as well as the allocation coefficients of ecological water use during key months (May–September), resulting in a total of 47 decision variables. The output variables of the surrogate model consist of two hydrological variables simulated by the coupled hydrological model (GSFLOW), namely the change in the average groundwater depth in the study area and the area of the terminal lake. For surrogate construction, Latin hypercube sampling was first applied to generate samples within the input variable space. Each sample set was then used as input to the GSFLOW model to obtain the corresponding outputs, thereby forming an input-output dataset. The dataset was subsequently randomly divided into a training set (70 %) and a test set (30 %). The training set was used to train the radial basis function neural network (RBF-NN), while the testing set was used to evaluate the predictive accuracy and generalization capability of the surrogate model.

## 4 Results

### 4.1 Calibration and validation of the basin-scale hydrological model with surrogate model assessment

Simulated daily runoff from the SRM model agrees well with observations, particularly during spring snowmelt, where both the timing and magnitude of peak flows are accurately captured. The SRM achieves Nash-Sutcliffe efficiency (NSE) values between 0.72 and 0.96, demonstrating its strong capability to accurately simulate seasonal snowmelt-driven runoff. These results demonstrate the SRM's capability in capturing the temporal variability of mountain inflows, making it suitable for providing reliable upstream boundary conditions to the GSFLOW model. The spatial distribution and numbering of the 22 sub-basins with available observations, as well as the corresponding SRM simulation results and comparisons with observed runoff, are shown in Figs. S1–S3 in the Supplement.

As shown in Fig. 3, GSFLOW simulations closely match observed monthly streamflow at Alar, Xinqiman, Yingbaza, Wusiman, and Qiala stations on the Tarim River main stem, with NSE values ranging from 0.6 to 0.7. This demonstrates that the model adequately represents runoff dynamics, including both high- and low-flow periods.

The agreement between observed and modeled groundwater levels at 139 monitoring wells throughout the validation period is shown in Fig. 4. The NSE of the groundwater simulation reached 0.96, demonstrating that the GSFLOW model can accurately capture groundwater dynamics at the observation points. It should be noted that the monitoring wells are unevenly distributed and limited in number, being mainly concentrated in the main stem of the Tarim River and the Hetian region.

The reliability of the GSFLOW model was further evaluated by comprehensive validation using multi-source remote sensing data, including evapotranspiration (ET), soil moisture (SM), and terrestrial water storage change (TWSC). The results of the comparison indicate that good overall consistency between model simulations and independent observations. Specifically, the simulated TWSC achieved an NSE of 0.66 against GRACE data, soil moisture an NSE of 0.61 against SM products, and evapotranspiration an NSE of 0.71 against the GLEAM dataset (see Figs. S6–S8). Collectively, these results indicate that the coupled SRM-GSFLOW model reliably simulates surface water-groundwater interactions in the Tarim River main stem, providing a robust hydrological foundation for optimizing agricultural and ecological water use.

The variation of the surrogate model's NRMSE and $R^2$ with the number of training samples is shown in Fig. S9. As the number of samples increases, the surrogate accuracy steadily improves. When 2842 samples are used, the coefficient of determination ($R^2$) reaches 0.98, corresponding to an

**Table 1.** Parameters related to crop planting management.

| Crop type | Market price (CNY $kg^{-1}$) | Irrigation quotas ($m^3\,hm^{-2}$) | Cultivation cost (CNY $hm^{-2}$) | Total nitrogen loading ($kg\,hm^{-2}$) |
|---|---|---|---|---|
| Maize | 2.0 | 5250 | 1463 | 339.7 |
| Cotton | 7.4 | 6750 | 1463 | 456.7 |
| Vegetable | 2.2 | 6750 | 1967 | 450.0 |
| Cucurbits | 3.6 | 5250 | 1967 | 350.0 |
| Fruit | 3.0 | 5250 | 1420 | 320.0 |
| Oilseed | 6.4 | 7350 | 1420 | 280.0 |

**Table 2.** The parameters of the NSGA-III.

| Parameter | Value |
|---|---|
| Population size ($N_{pop}$) | 300 |
| Maximum number of generations ($G_{max}$) | 6000 |
| Crossover probability ($P_c$) | 0.9 |
| Mutation probability ($P_m$) | 0.05 |
| Epsilon resolution | (1.0, 0.01, 0.001) |

**Table 3.** Annual runoff ranges under different hydrological years.

| Grade | Anomaly percentage $P/\%$ | Mainstream Inflow ($108\,m^3$) |
|---|---|---|
| Wet Year | $P<37.5$ | $W>63.93$ |
| Normal Year | $37.5 \le P \le 87.5$ | $39.53 \le K \le 63.93$ |
| Dry Year | $P > 87.5$ | $W < 39.53$ |

NRMSE of 0.016. Additionally, a five-fold cross-validation was conducted to assess overfitting risk; the results are summarized in Table S2 in the Supplement, which shows consistent RMSE across folds.

### 4.2 Optimization Multi-objective optimization results

#### 4.2.1 Pareto-optimal solutions

A multi-objective management model based on the NSGA-III algorithm was developed, incorporating four objective functions, namely agricultural economic benefit per unit of irrigation water ($f_{AB}$), average cumulative groundwater level rise ($f_{GL}$), surface area of Taitema Lake ($f_{L_A}$), and total nitrogen load from agricultural non-point sources ($f_{TN}$).

Hydrological conditions were classified as wet, normal, or dry years based on the runoff anomaly percentage ($P$), as defined in Table 3. The years 2010, 2016, and 2009 were selected as representative dry, normal, and wet years, respectively.

To reveal trade-offs among objectives and their variation with hydrology, parallel coordinate plots of Pareto-optimal solutions were generated for wet, normal, and dry years (Fig. 5a–c). In these plots, each objective is represented as a parallel axis, and each polyline corresponds to an optimal management strategy, illustrating interactions and trade-offs among objectives.

The patterns in the parallel coordinate plots show an overall positive correlation between $f_{AB}$ and $f_{TN}$, indicating that higher agricultural economic benefits generally coincide with increased nitrogen fertilizer use and heightened non-point source pollution. In contrast, both $f_{GL}$ and $f_{L_A}$ exhibit negative correlations with $f_{AB}$. Under a fixed total surface water inflow, expansion of agricultural water use tends to crowd out ecological water allocations, leading to simultaneous declines in groundwater recovery and terminal lake area. This highlights the inherent competition for limited water resources among agricultural production, groundwater sustainability, and terminal lake ecosystem restoration.

Across hydrological scenarios, the Pareto frontier is most expansive in wet years, indicating greater system flexibility and management space under abundant water, where conflicts among objectives are relatively weaker. In normal years, solution sets become more concentrated, reflecting a more balanced but constrained trade-off structure. In dry years, the Pareto solution space narrows substantially, and overall objective values decline, with $f_{L_A}$ decreasing by approximately 30 % compared to normal years, underscoring the strong dependence of terminal lake ecological inflows on hydrological conditions.

Nonlinear trade-offs are also evident, particularly between $f_{GL}$ and $f_{AB}$ and between $f_{GL}$ and $f_{L_A}$, where the parallel coordinate plots show segments with distinct slopes. This indicates that increases in agricultural irrigation exert nonlinear impacts on groundwater levels and lake inflows, and that the multi-objective system is highly sensitive to changes in management strategies.

Overall, agricultural water use expansion enhances regional economic output but simultaneously exacerbates groundwater depletion and terminal lake degradation, reflecting the intrinsic trade-offs within the water-ecology-agriculture nexus.

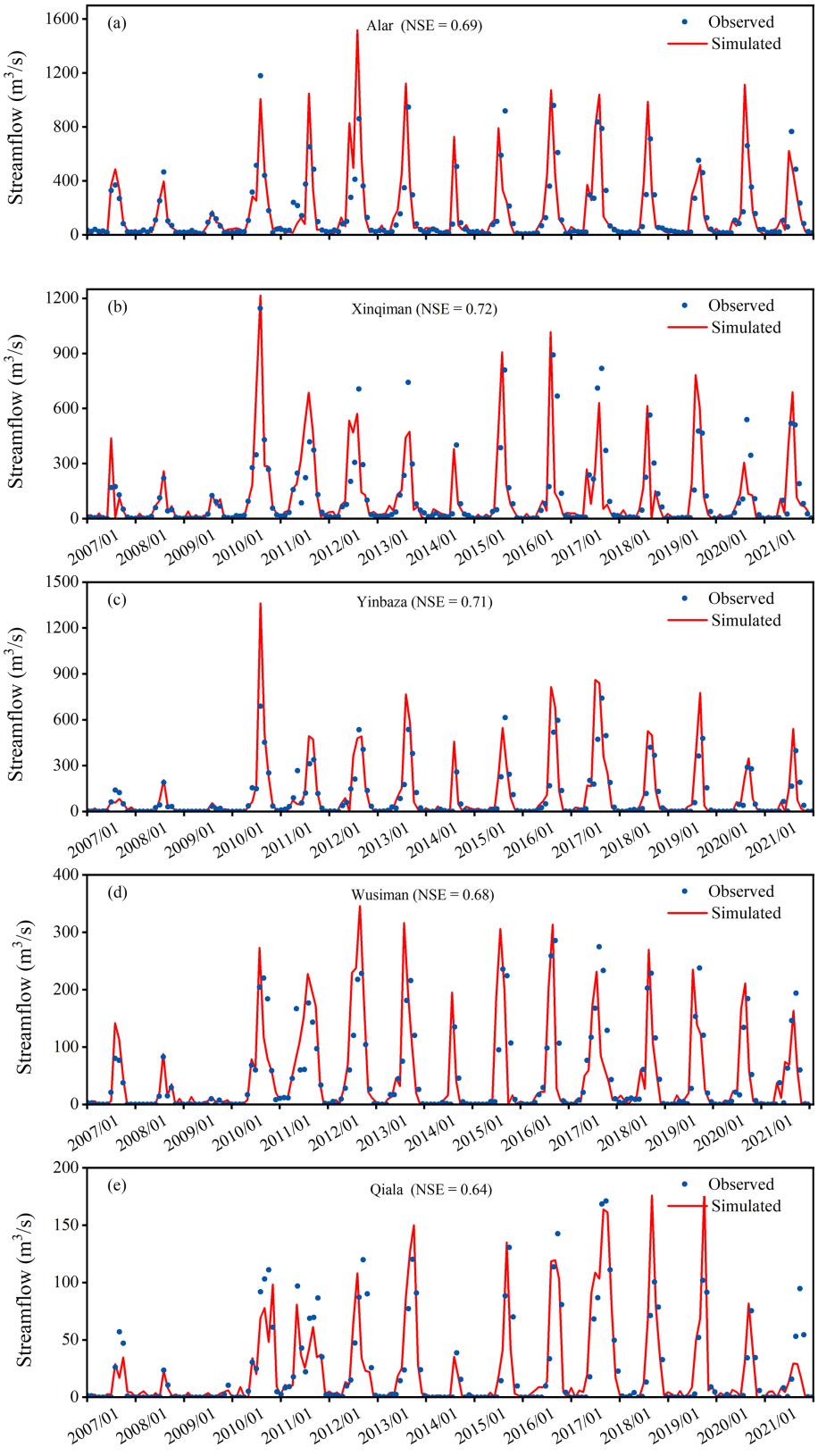


**Figure 3. (a)–(e)** present the evaluation of monthly streamflow simulations against observations at Alar and Xinqiman, Yingbaza, Wusiman, and Qiala gauging stations, respectively.

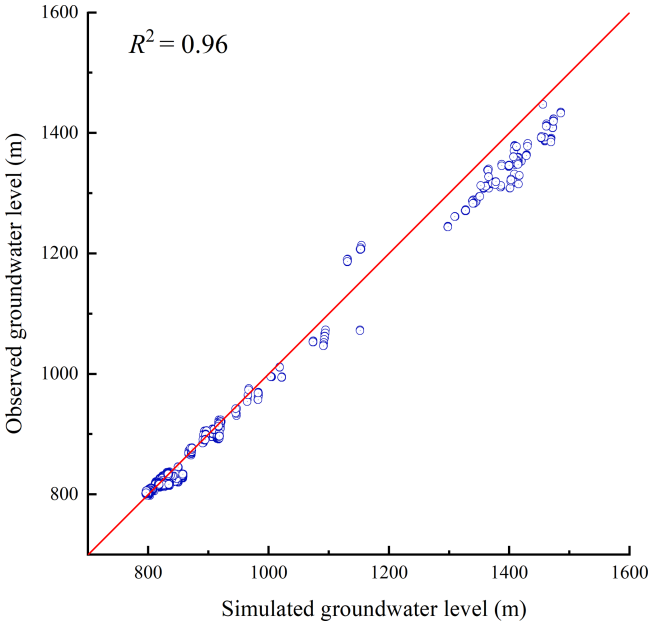


**Figure 4.** The evaluation of simulated groundwater levels against observations during the validation period.

#### 4.2.2 Comparison of representative solutions and multi-objective trade-offs

To systematically evaluate trade-offs among agricultural economic benefit, groundwater security, ecological water allocation, and nitrogen pollution, five representative solutions were selected from the Pareto-optimal set under each hydrological scenario (dry, normal, and wet), resulting in a total of 15 solutions. These solutions include the solution with maximum agricultural economic benefit (S1, S6, S11), the solution with maximum groundwater level rise (S2, S7, S12), the solution with maximum terminal lake area (S3, S8, S13), the solution with minimum total nitrogen load (S4, S9, S14), and the compromise solution with the most balanced overall performance (S5, S10, S15). The compromise solutions were identified using the Technique for Order Preference by Similarity to Ideal Solution (TOPSIS), where normalized objective values were compared against ideal and negative-ideal solutions, and the solution closest to the ideal and farthest from the negative-ideal was selected. Additionally, the Pareto sets were projected onto two-dimensional planes defined by $f_{AB} - f_{GL}$, $f_{GL} - f_{L_A}$, and $f_{AB} - f_{TN}$ to illustrate synergies and conflicts among the objectives.

Figures 6–8 show the Pareto-optimal solution distributions corresponding to dry, normal, and wet hydrological scenarios. Across all scenarios, a mild trade-off exists between $f_{AB}$ and $f_{GL}$. High-benefit solutions (e.g., S6, S9, S11) typically correspond to slightly lower groundwater recovery, reflecting a greater allocation of water to agriculture at the expense of ecological replenishment.

Apparently, $f_{AB}$ shows a pronounced negative correlation with $f_{L_A}$ under all hydrological conditions. For example, in the dry year scenario, solution S1 achieves the highest agricultural economic benefit (CNY 2.52 $m^{-3}$) but results in a relatively small lake area (85.32 $km^2$). In contrast, the ecological priority solution S3 produces a slightly lower $f_{AB}$ (CNY 2.38 $m^{-3}$) while achieving the largest $f_{L_A}$ (93.20 $km^2$). This indicates that upstream irrigation expansion directly reduces downstream ecological water availability, a pattern particularly pronounced in dry years.

Generally, $f_{TN}$ increases with $f_{AB}$, although notable differences exist among individual solutions. In the wet year scenario, the compromise solution S15 yields a $f_{AB}$ of CNY 2.38 $m^{-3}$ with a corresponding $f_{TN}$ of $0.70 \times 108$ kg $yr^{-1}$, which is lower than solution S12 ($f_{AB}$ = CNY 2.30 $m^{-3}$, $f_{TN} = 0.74 \times 108$ kg $yr^{-1}$). This suggests that even when prioritizing economic output, non-point source pollution can be mitigated through appropriate management. Nevertheless, the overall trend confirms that higher agricultural benefits generally rely on greater fertilizer inputs, highlighting a persistent conflict between production and environmental protection. This conflict necessitates coordinated management through precision fertilization and optimized crop structure.

Comparing the compromise solutions (S5, S10, S15) across scenarios further reveals their scenario-dependent nature. In the dry year (S5), moderate agricultural benefits (CNY 2.43 $m^{-3}$) are achieved alongside relatively high ecological water supply (90.88 $km^2$) and low nitrogen load ($0.47 \times 108$ kg $yr^{-1}$). In the normal year (S10), a more balanced combination of economic and ecological benefits is obtained ($f_{AB}$ = CNY 2.47 $m^{-3}$, $f_{L_A} = 95.32$ $km^2$), while maintaining a low nitrogen load ($0.54 \times 108$ kg $yr^{-1}$). In the wet year (S15), $f_{AB}$ (CNY 2.38 $m^{-3}$) remains at an intermediate level, with $f_{L_A}$ (95.75 $km^2$) and $f_{GL}$ (1.52 m) also showing moderate performance, and $f_{TN}$ ($0.70 \times 108$ kg $yr^{-1}$) remaining lower than that the solutions S12. These results reflect a clear compromise, rather than the comprehensive optimization of any single objective. The detailed values of all representative solutions, including compromise solutions, are summarized in Table 4.

Overall, compromise solutions achieve relatively balanced performance across conflicting objectives, but this balance comes at the cost of sacrificing optimal performance in any single objective. Comparisons across hydrological scenarios show that management flexibility is greatest in wet years, while multi-objective conflicts intensify during dry years, when trade-offs between agricultural expansion and ecological water requirements become particularly pronounced.

#### 4.2.3 Suitable cultivated land area

Table 5 presents the suitable cultivated land area ranges and corresponding optimal cropping structures under different hydrological scenarios. Suitable cultivation scale varies

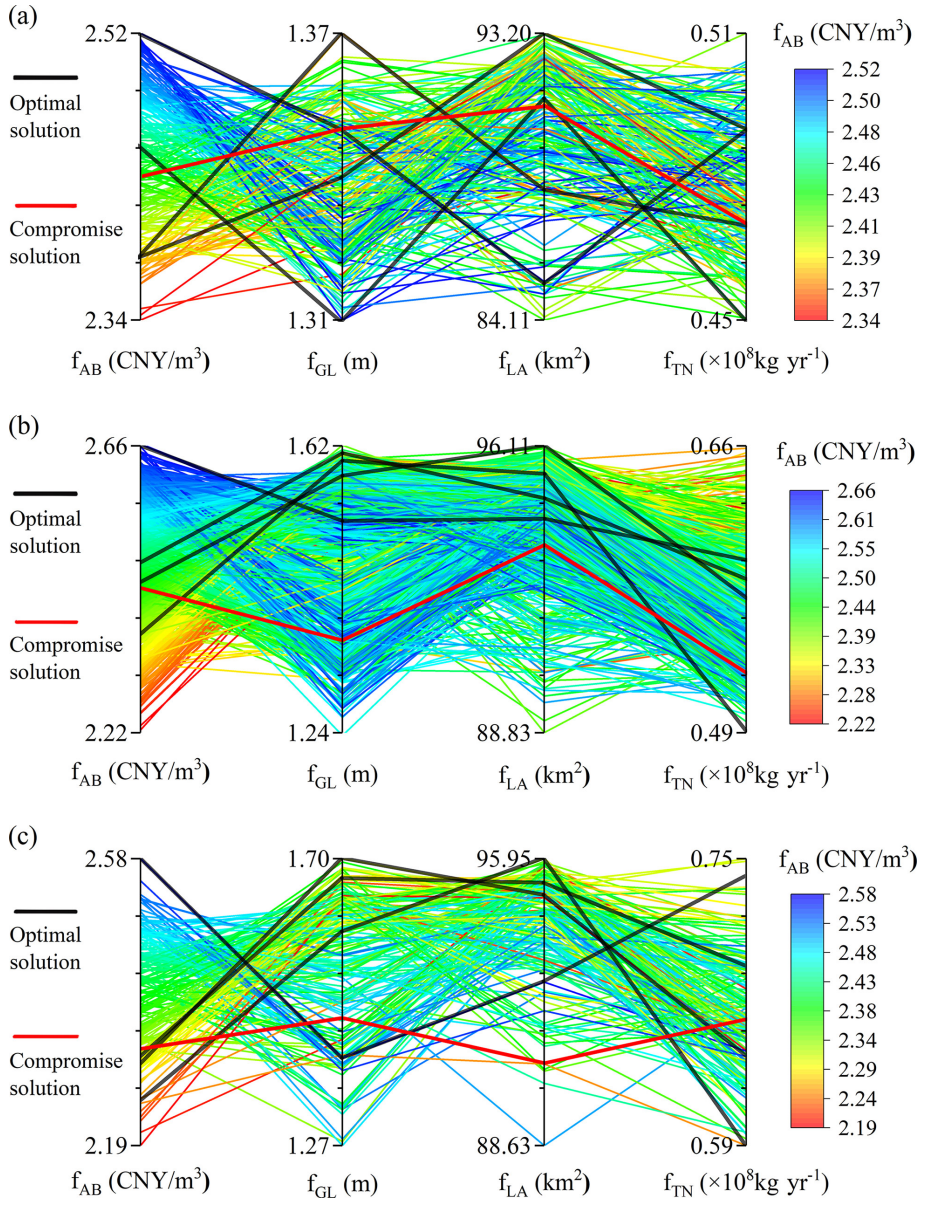


**Figure 5.** Objective values ($y$ axis) plotted against management objectives $f_{AB}$, $f_{GL}$, $f_{L_A}$ and $f_{TN}$, with panels **(a)**, **(b)**, and **(c)** representing dry, normal, and wet years, respectively.

substantially across hydrological conditions. The suitable cultivated area ranges from $11.3 \times 104$–$14.3 \times 104\,hm^2$ in wet years, declines to $10.1 \times 104$–$13.1 \times 104\,hm^2$ in normal years, and contracts further to $9.5 \times 104$–$11.9 \times 104\,hm^2$ in dry years. These results demonstrate that available water is the primary constraint on regional agricultural scale.

Comparing optimal cropping structures across scenarios reveals that improved water availability favors allocating land to high-benefit crops. The proportions of vegetables and melons increase steadily, rising by 3.11 % and 0.72 %, respectively, in wet versus dry years, whereas those of maize and oil crops decline. The proportion of fruit crops decreases to 7.56 % in wet years (down 1.64 % from dry years), reflecting their heightened sensitivity to ecological and water quality constraints in multi-objective trade-offs. Overall, the optimized cropping structures achieve a coordinated balance between cultivated land scale and water resource utilization through adjustments in crop composition.

Figure 9a–c show the spatial distribution of suitable cultivated land area across the study regions under dry, normal, and wet hydrological scenarios. Under dry conditions (Fig. 9a), cultivated land area shows pronounced spatial heterogeneity. In the upstream area, Zone 1 has the most stable cultivated area ($3.30$–$4.30 \times 104\,hm^2$), significantly larger

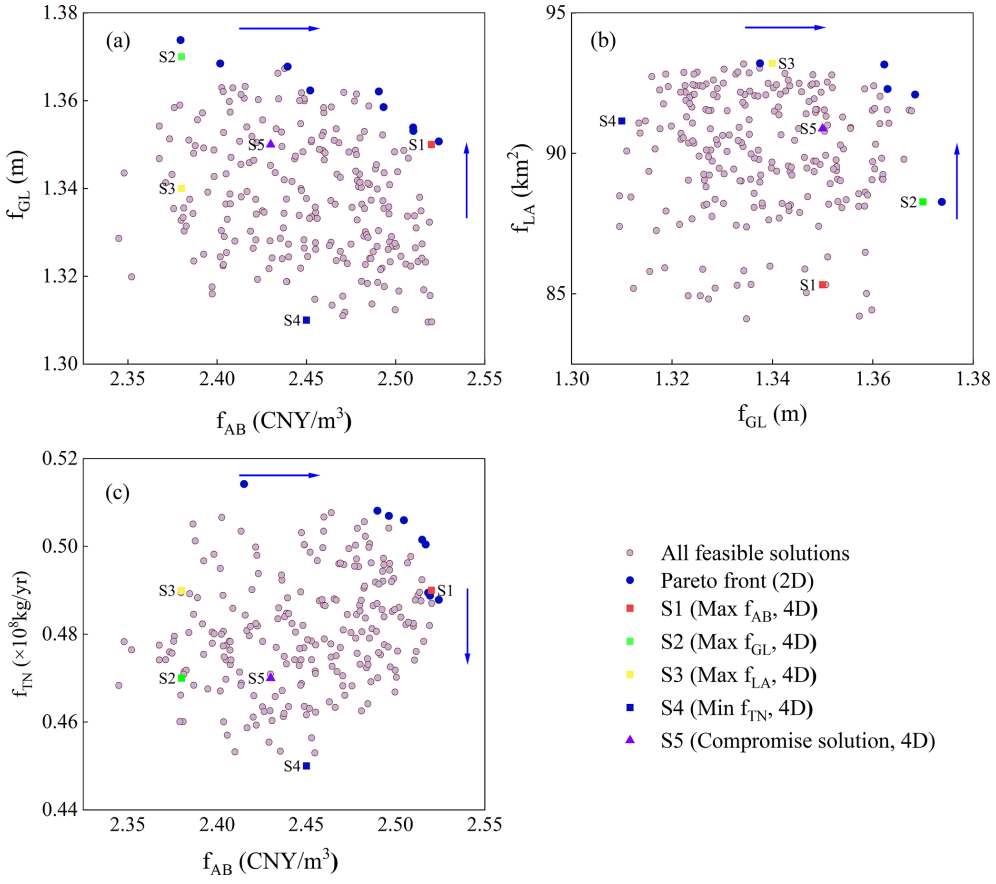


**Figure 6.** Scatter plots for optimization in a dry year exhibiting the correlation between each pair of objectives, **(a)** $f_{AB}$ and $f_{GL}$; **(b)** $f_{GL}$ and $f_{LA}$; and **(c)** $f_{AB}$ and $f_{TN}$. Each dot represents a feasible solution. The representative solutions for dry scenario (S1–S5) can be identified by rectangles with different color. The navy-blue arrow indicates the direction of Pareto optimality.

**Table 4.** Objective values for each of the 15 solutions.

| Scenario | Solutions | $f_{AB}$ (CNY m$^{-3}$) | $f_{GL}$ (m) | $f_{LA}$ (km$^2$) | $f_{TN}$ ($\times 10^8$ kg yr$^{-1}$) |
|---|---|---|---|---|---|
| Dry | S1 | 2.52 | 1.35 | 85.32 | 0.49 |
| | S2 | 2.38 | 1.37 | 88.27 | 0.47 |
| | S3 | 2.38 | 1.34 | 93.20 | 0.49 |
| | S4 | 2.45 | 1.31 | 91.15 | 0.45 |
| | S5 | 2.43 | 1.35 | 90.88 | 0.47 |
| Normal | S6 | 2.66 | 1.52 | 94.25 | 0.54 |
| | S7 | 2.48 | 1.61 | 94.77 | 0.59 |
| | S8 | 2.45 | 1.58 | 96.11 | 0.58 |
| | S9 | 2.48 | 1.32 | 92.79 | 0.50 |
| | S10 | 2.47 | 1.44 | 95.32 | 0.54 |
| Wet | S11 | 2.58 | 1.40 | 92.80 | 0.64 |
| | S12 | 2.30 | 1.70 | 95.01 | 0.74 |
| | S13 | 2.31 | 1.59 | 95.95 | 0.66 |
| | S14 | 2.25 | 1.40 | 90.69 | 0.59 |
| | S15 | 2.38 | 1.52 | 95.75 | 0.70 |

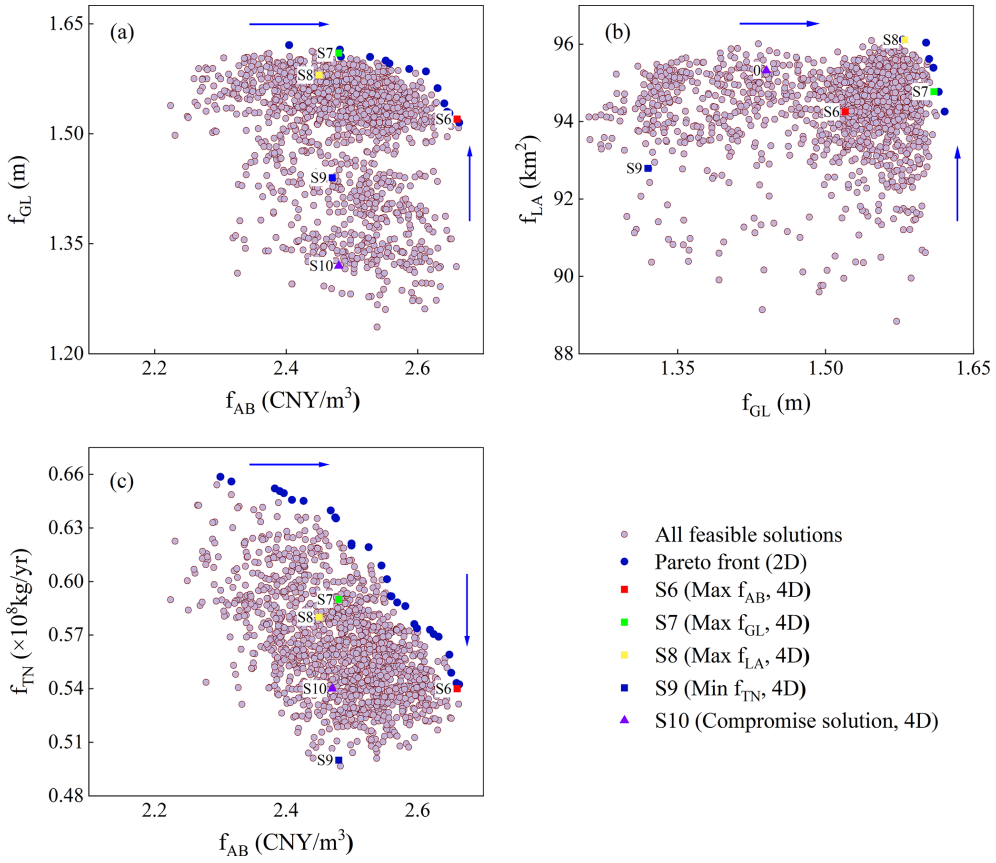


**Figure 7.** Scatter diagrams depicting correlations among objective pairs in a normal year, **(a)** $f_{AB}$ and $f_{GL}$; **(b)** $f_{GL}$ and $f_{LA}$; and **(c)** $f_{AB}$ and $f_{TN}$. Representative normal-year solutions (S6–S10) are marked using colored rectangles.

**Table 5.** Optimal crop structure proportions and suitable cultivated land area under different hydrological scenarios.

| Hydrological Year | Suitable Cultivated Area (104 hm$^2$) | Maize | Cotton | Vegetables | Melons | Oilseed | Fruits |
|---|---|---|---|---|---|---|---|
| Dry Year | 9.5–11.9 | 2.84 | 75.84 | 1.71 | 1.71 | 2.72 | 9.2 |
| Normal Year | 10.1–13.1 | 4.68 | 69.83 | 2.48 | 2.69 | 3.25 | 11.23 |
| Wet Year | 11.3–14.3 | 6.58 | 69.72 | 4.82 | 2.43 | 4.15 | 7.56 |

than that of the most water-constrained Zone 4 (approximately 0.26–0.39 × 104 hm$^2$). In the midstream, Zones 5 and 6 show the widest fluctuation ranges, indicating high sensitivity to trade-offs. In the downstream area, Zone 7 shows a marked contraction in scenarios prioritizing ecological objectives.

Under normal conditions (Fig. 8b), cultivated land area increases in all regions relative to dry years. In the upstream area, Zone 3 exhibits substantial variability (1.09 × 104–1.83 × 104 hm$^2$), indicating that its cultivated area is strongly co-determined by crop structure adjustments and water availability. In the midstream area, Zone 6 expands notably, whereas downstream Zone 7 remains tightly constrained by ecological water demands.

Under wet conditions (Fig. 9c), the land's carrying capacity for agriculture increases markedly. The downstream Zone 7 responds most strongly, reaching 3.84 × 104 hm$^2$ in solution S12, indicating substantial expansion potential. However, the upstream Zone 3 shows contraction under ecology-oriented or water-quality-oriented solutions, indicating that ecological objectives remain binding constraints even under abundant water conditions.

Overall, regional variation in suitable cultivated area is jointly shaped by hydrological conditions and management preferences. Cultivated area must contract during dry years but can expand in wet years. The midstream area is most sensitive to trade-offs, while the downstream area has the greatest expansion potential in wet years. These findings confirm

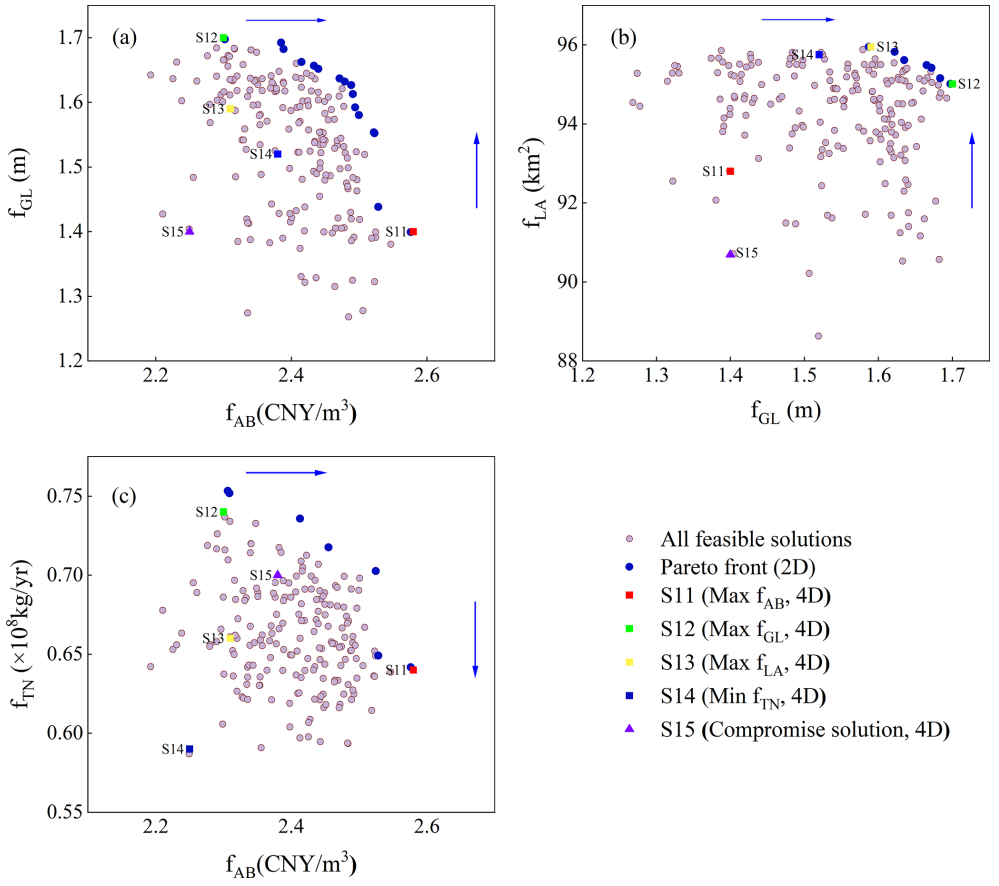


**Figure 8.** Scatter diagrams depicting correlations among objective pairs under a wet year, **(a)** $f_{AB}$ and $f_{GL}$; **(b)** $f_{GL}$ and $f_{LA}$; and **(c)** $f_{AB}$ and $f_{TN}$. Representative wet-year solutions (S11–S15) are marked using colored rectangles.

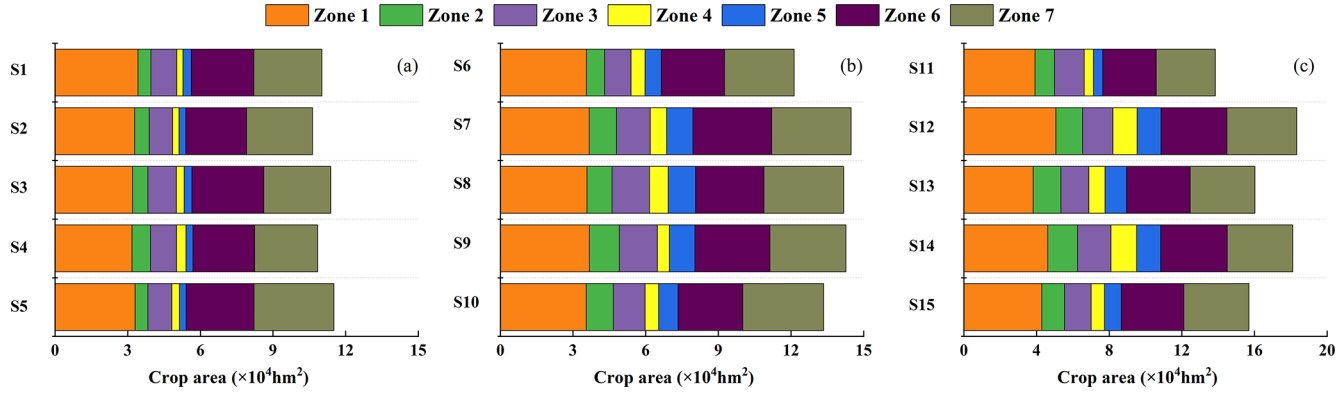


**Figure 9.** Suitable cultivated land area in each region under different hydrological scenarios.

that hydrological conditions dominate agricultural scale regulation, and that multi-objective optimization offers feasible pathways to balance economic and ecological objectives.

#### 4.2.4 Crop structure optimization based on multi-objective trade-offs

Based on the identified suitable land scales, this section examines how optimal cropping structures adjust to different hydrological conditions. Figure 10 presents the optimal cropping structures corresponding to solutions S1–S15.

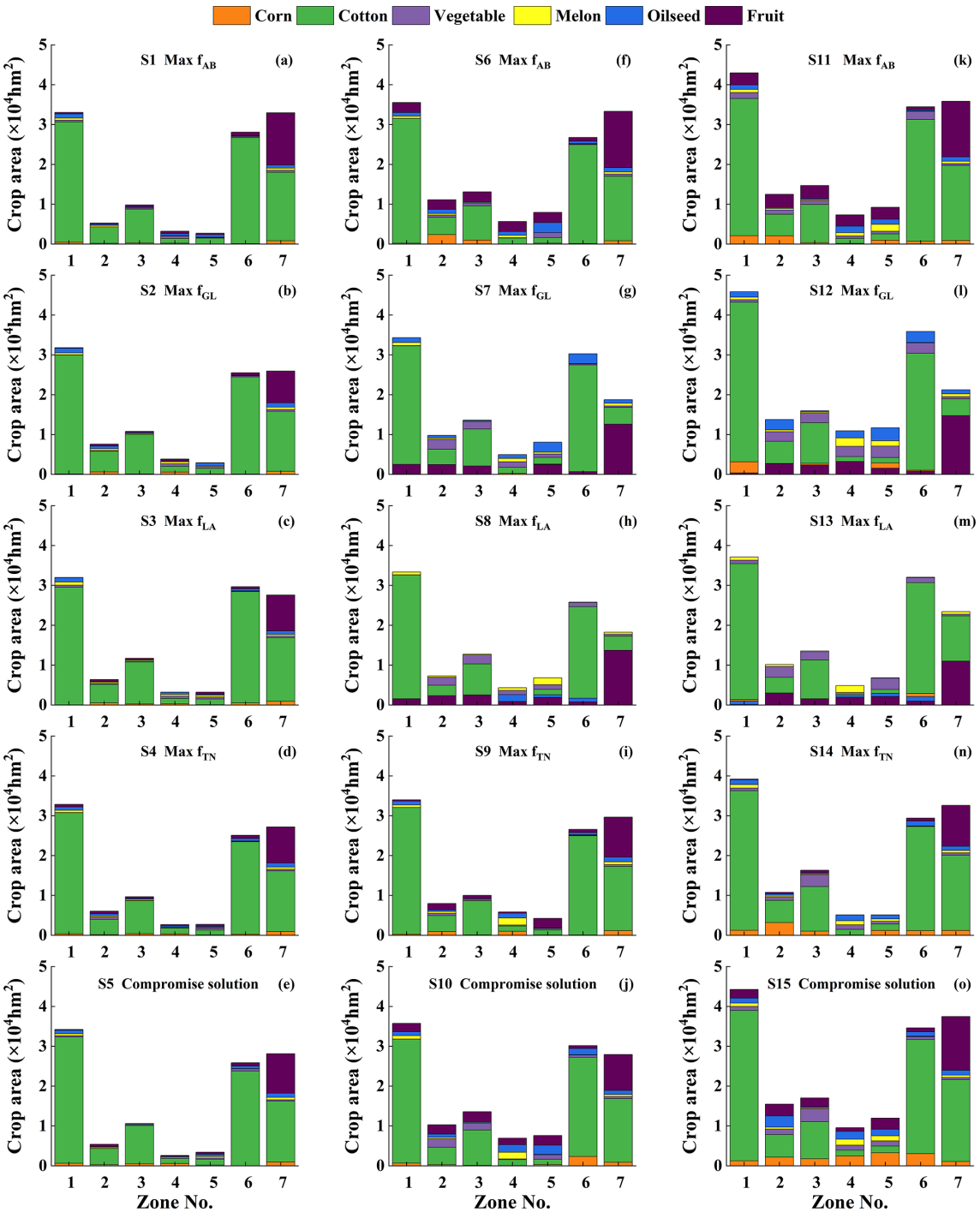


**Figure 10.** Crop planting structures (corn, cotton, vegetable, melon, oilseed and fruit) for the selected solutions (S1–S15), with panels **(a)–(e)**, **(f)–(j)**, **(k)–(o)** representing dry, normal, and wet years, respectively.

As total irrigation demand rises from 110.75 to 136.98 × 108 $m^3$ from dry to wet years, cropping structures adjust systematically. High-benefit crops expand continuously, with the proportion of vegetables increasing by 3.11 % and that of melons rising slightly by 0.72 %, while the proportion of fruit crops decreases by 1.64 %. This pattern indicates that, under multi-objective constraints, crop allocation increasingly emphasizes integrated economic and environmental performance. In contrast, maize and oil crop proportions rise slightly in wet years, suggesting they retain a competitive advantage when water is plentiful.

In dry years (S1–S5), the proportions of cotton and vegetables decline markedly across all regions, while maize and oil crops account for a relatively larger share. In Zones 4–7, the cultivated area of water-intensive melon crops is substantially restricted to reduce pressures on downstream ecological water demands.

Ecological protection objectives are a key constraint on cropping structure. In dry years, water-intensive melon cultivation in the midstream and downstream regions (Zones 4–7) is strictly limited to safeguard downstream ecological baseflows. Even in wet years with relatively abundant water, the expansion of water-intensive melons and fruit trees in downstream Zones 6–7 remains limited to avoid excessive irrigation demand during critical ecological windows, such as the germination of Populus euphratica forests.

As shown in Table 6, total nitrogen input increases from $4.71 \times 104$ t in dry years to $5.87 \times 104$ t in wet years, broadly tracking the expansion of cultivated land area and without pronounced spatial concentration. This indicates that the optimized cropping structures achieve a relatively even distribution of nitrogen fertilizer inputs, effectively avoiding localized intensification of environmental risks.

In summary, the optimal cropping structure is a dynamic system that flexibly adjusts crop composition to hydrological variability while respecting ecological thresholds.

## 5 Discussion

### 5.1 Implications for coordinated water-agriculture-ecosystem management in arid river basins

This study develops a multi-objective water-ecosystem-agriculture (WEA) optimization framework to systematically elucidate the coordination between cropping structure adjustment and water allocation in the Tarim River mainstream. The results reveal pronounced trade-offs between agricultural economic benefits ($f_{\mathrm{AB}}$) and ecological objectives ($f_{L_A}$ and $f_{\mathrm{GL}}$), as well as environmental objectives ($f_{\mathrm{TN}}$), confirming the widely recognized "water-food-ecosystem" dilemma in arid inland river basins (Li et al., 2024). Compared with the ecological crises driven by upstream-downstream water competition in the Aral Sea Basin (Azimov and Avezova, 2022), the multi-objective optimization approach adopted here provides a quantitative tool to explicitly characterize and manage such conflicts.

Notably, conflicts between $f_{\mathrm{AB}}$ and ecological objectives ($f_{\mathrm{GL}}$, $f_{L_A}$) can be mitigated through scientifically designed adjustments to cropping structure and irrigation practices. This suggests that sustaining agricultural output can be compatible with ecological preservation, providing fresh perspectives for managing water resources in arid regions.

Hydrological conditions strongly regulate system-level trade-offs. During dry years, system resilience declines markedly and multi-objective conflicts intensify, consistent with observations from the Aral Sea Basin where upstream-downstream tensions are exacerbated under drought conditions (Saidmamatov et al., 2020). In contrast, wet years provide greater management flexibility and create critical windows of opportunity for achieving multi-objective coordination through structural adjustment rather than rigid water allocation constraints.

The compromise solutions identified in this study exhibit robust overall performance across different hydrological scenarios. Their strength lies in shifting the paradigm from a "win-lose" trade-off toward a more balanced "shared-benefit" outcome. For example, under dry-year conditions, solution S5 maintains moderate agricultural economic returns while effectively safeguarding ecological water requirements and controlling nitrogen pollution risks. This structurally optimized pathway aligns with recent practical efforts in the adjacent Yanqi Basin, where cropping structure adjustment has been used to achieve simultaneous economic and ecological gains (Tang et al., 2024). The present study further strengthens such empirical findings by providing quantitative, system-level evidence.

Spatial heterogeneity analysis underscores the necessity of differentiated management strategies. The midstream area exhibits the highest sensitivity to multi-objective trade-offs and thus requires more refined water-use regulation. Although the downstream area shows expansion potential during wet years, strict adherence to ecological thresholds remains essential. These findings are highly consistent with the differentiated management principles embodied in Xinjiang's "Three Red Lines" water policy (Tao et al., 2012).

Dynamically optimizing cropping structure is a key pathway to multi-objective coordination. As hydrological conditions improve, the proportion of high-benefit crops can be moderately increased, but such adjustments must remain firmly constrained by ecological safety considerations. In downstream ecologically sensitive zones, even under relatively abundant water availability, the expansion of high water-consuming crops should be strictly limited. This "ecology-first" optimization principle is critical for maintaining long-term ecological security in arid river basins.

Compared to previous studies in the Tarim River Basin that primarily focused on single or dual objectives, the multi-objective optimization framework developed in this study provides a more comprehensive analytical approach for coordinating WEA conflicts. By integrating a coupled surface water-groundwater model with multi-objective decision-making methods, this framework transforms ecological responses from static constraints into optimization objectives that can be dynamically adjusted with management strategies. This approach enhances the ability to characterize the relationship between agricultural water use and ecological feedback. Although simplifications in the coupled hydrological model are inevitable, it still provides a

**Table 6.** Agricultural area, water demand, and nitrogen input under representative scenarios.

| Hydrological Year | Total Cultivated Area ($10^4$ hm$^2$) | Total Water Demand (108 m$^3$) | Total Nitrogen Input ($10^3$ t) |
|---|---|---|---|
| Dry Year (S5) | 11.02 | 110.75 | 4.71 |
| Normal Year (S10) | 12.14 | 121.21 | 5.19 |
| Wet Year (S15) | 13.85 | 136.98 | 5.87 |

more structured cognitive perspective for analyzing trade-offs within the WEA system.

When this method is to be extended to other basins, its applicability does not depend on the simple transplantation of models or data, but on the ability to implement spatially differentiated management according to local conditions. For example, in regions lacking hydrogeological data, a more generalized hydrological model could be used to represent water cycle processes. When the accuracy of crop spatial distribution data is limited, statistical data can be used to impose total area constraints at the regional scale. Furthermore, attention should be paid to uncertainty factors that significantly influence the optimization results (such as key hydrogeological parameters and agricultural management parameters), and their impact on decision-making outputs should be quantified through sensitivity analysis to provide necessary risk warnings for practical applications. The research framework presented in this study may provide useful insights for other basins facing similar water resource challenges, although it should be further adapted and validated according to local conditions.

### 5.2 Limitations of the study

The practical feasibility of the optimized solutions requires further field validation. Owing to the lack of long-term, large-scale monitoring data that simultaneously capture cropping structure adjustment and ecological water conveyance processes, the real-world applicability of the identified Pareto-optimal solutions remains uncertain. Future research should integrate data from ecological water regulation projects and water-saving agriculture demonstration programs to further calibrate and validate model outputs.

Multiple sources of uncertainty have not yet been systematically quantified or propagated through the optimization process. Key inputs, including climate forcing data, hydrogeological parameters, crop water requirement coefficients, and fertilizer-related parameters, all contain uncertainties that may accumulate and propagate step by step, affecting the shape and range of the Pareto front as well as the stability of compromise solutions. In addition, scale transformation during model construction – coupling basin-scale hydrological simulations with grid-based land use and crop distribution data – introduces errors from spatial scaling and parameter aggregation that are difficult to fully quantify. The influence of future climate change on runoff patterns and crop water requirements has also not been explicitly addressed. Additionally, the proportional adjustment method used for groundwater abstraction represents a simplified treatment. When the intensity or spatial distribution of groundwater abstraction changes significantly, the model should be updated and recalibrated using the latest statistical data to ensure the reliability of simulation and prediction results. Future research may introduce a Hierarchical Bayesian Model (Wu et al., 2010) to quantify and control the impacts of different uncertainty sources on optimization solutions, providing more robust management strategies for decision makers. Including climate change scenarios constitutes another key avenue for future studies.

This study employs the Export Coefficient Model to estimate agricultural nitrogen loads. This method offers high computational efficiency for strategic, long-term analyses at the watershed scale, making it suitable for the rapid assessment of pollution risks under multiple scenarios. However, as a static, spatially lumped empirical model, it is inherently limited in its ability to accurately describe the transport and transformation processes of nitrogen within the soil-groundwater system and their spatial heterogeneity under different irrigation or fertilization regimes. Therefore, the model is better suited for comparative analysis and relative risk assessment among different management schemes, rather than for the precise, process-based quantification and prediction of pollution.

Although the GSFLOW model can simulate coupled surface water-groundwater processes, its representation of vegetation mainly relies on predefined crop coefficients and canopy parameters, which makes it difficult to fully capture the spatiotemporal dynamics of vegetation growth and their influence on the hydrological cycle. Recent studies have shown that assimilating satellite-derived vegetation indices (e.g., Leaf Area Index, LAI) into hydrological models can significantly improve simulations of evapotranspiration, soil moisture, and groundwater recharge. For example, studies by Paul et al. (2021), Bian et al. (2019), and Li et al. (2009) demonstrated that assimilating MODIS-LAI data can effectively improve watershed-scale runoff and evapotranspiration simulations. At the irrigation district scale, Zafarmomen et al. (2024) further showed that assimilating high-resolution Sentinel-2 LAI into hydrological models can more accurately represent the effects of vegetation dynamics on

evapotranspiration, irrigation return flows, and groundwater recharge, thereby improving the simulation of surface water-groundwater interactions. Future research could build upon these approaches by assimilating multi-source remote sensing LAI data into the coupled modeling framework used in this study, thereby improving the representation of hydrological processes, particularly the effects of ecological water replenishment, and providing more reliable distributed hydrological state information for multi-objective optimization. The application of higher-resolution process-based models could further enhance the precision and reliability of system simulations.

## 6 Conclusions

A coordinated water-ecosystem-agriculture (WEA) management framework is critical for alleviating conflicts between ecological degradation and agricultural development in arid inland river basins. Focusing on the mainstream region of the Tarim River Basin as a case study, this research constructs a coupled hydrology-agriculture multi-objective optimization model to systematically characterize trade-offs among multiple objectives and to propose strategies for coordinated WEA management. The main conclusions are summarized as follows.

Multi-objective optimization demonstrates pervasive trade-offs within the WEA system. Significant trade-offs are observed among agricultural economic benefit ($f_{\mathrm{AB}}$), terminal lake area ($f_{L_A}$), and total nitrogen load ($f_{\mathrm{TN}}$). Solutions that maximize economic output achieve higher agricultural returns at the cost of reduced ecological water availability and increased nitrogen pollution, whereas solutions emphasizing ecological or environmental objectives require moderate reductions in agricultural output. These results indicate that strategies solely focused on agricultural expansion are unsustainable and underscore the need for systematic balancing of multiple objectives.

Spatially differentiated regulation based on regional heterogeneity effectively balances water, ecological, and agricultural objectives. Upstream irrigation districts, benefiting from relatively stable water availability, maintain higher levels of agricultural production under multi-objective trade-offs. By contrast, midstream and downstream areas are highly sensitive to ecological water level and conveyance constraints, resulting in larger fluctuations in agricultural scale and stricter restrictions on the expansion of water-intensive crops. These results underscore the need for management strategies tailored to the specific conditions of arid river basins.

Under multi-objective optimization, cropping structures can be dynamically adjusted to coordinate cultivated land scale and crop composition. Cotton consistently dominates the optimized cropping structure (69.72 %–75.84 %), providing stability to regional agricultural economic performance. Cropping structures respond dynamically to hydrological conditions. During wet years, the cultivated land area can be moderately expanded to $11.3 \times 104$–$14.3 \times 104\,\mathrm{hm}^2$, with greater allocation to high-value crops, including vegetables. In contrast, during dry years, cultivated land must be reduced to $9.5 \times 104$–$11.9 \times 104\,\mathrm{hm}^2$, placing more emphasis on water-saving crops such as maize and oil crops, while strictly limiting the planting of high water-consuming crops in midstream and downstream areas. This optimized configuration ensures coordinated management of cultivated land scale, crop structure, and nitrogen inputs, thereby preventing localized intensification of environmental risks.

*Data availability.* The ERA5 reanalysis precipitation data (Hersbach et al., 2020) can be downloaded from https://doi.org/10.24381/cds.e2161bac (Copernicus Climate Change Service, 2019). The GLEAM_v3.5a data (Martens et al., 2017; Miralles et al., 2011) is available at https://www.gleam.eu/ (last access: 17 June 2026). The GRACE RL06 Center for Space Research (https://doi.org/10.5067/TEMSC-3JC63, CSR, 2023) mascon products (Save et al., 2016) can be acquired from https://www2.csr.utexas.edu/grace/RL06_mascons.html (last access: 17 June 2026). Monthly streamflow data simulated by the SRM model have been made publicly available via the zenodo platform (https://doi.org/10.5281/zenodo.18151460, Zeng and Chen, 2025).

*Supplement.* The supplement related to this article is available online at https://doi.org/10.5194/hess-30-3741-2026-supplement.

*Author contributions.* Conceptualization, X.Z.; data collection, D.C; methodology, D.C. and X.Z.; validation, D.C. and X.Z.; writing-original draft preparation, D.C.; writing-review and editing, D.C. and X.Z.; supervision, D.G., D.W. and J.W.; project administration, D.G., D.W. and J.W.. All authors have read and agreed to the published version of the manuscript.

*Competing interests.* The contact author has declared that none of the authors has any competing interests.

*Disclaimer.* Publisher's note: Copernicus Publications remains neutral with regard to jurisdictional claims made in the text, published maps, institutional affiliations, or any other geographical representation in this paper. The authors bear the ultimate responsibility for providing appropriate place names. Views expressed in the text are those of the authors and do not necessarily reflect the views of the publisher.

*Acknowledgements.* The authors thank the High-Performance Computing Center (HPCC) of Nanjing University for providing computational platform support for this study.

*Financial support.* This research has been supported by the National Natural Science Foundation of China, Major Research Plan (grant no. 42477082).

*Review statement.* This paper was edited by Yonggen Zhang and reviewed by three anonymous referees.

## References

Avellán, T., Ardakanian, R., Perret, S. R., Ragab, R., Vlotman, W., Zainal, H., Im, S., and Gany, H. A.: Considering resources beyond water: irrigation and drainage management in the context of the water-energy-food nexus, Irrig. Drain., 67, 12–21, https://doi.org/10.1002/ird.2154, 2018.

Azimov, U. and Avezova, N.: Sustainable small-scale hydropower solutions in central Asian countries for local and cross-border energy/water supply, Renew. Sust. Energ. Rev., 167, 112726, https://doi.org/10.1016/j.rser.2022.112726, 2022.

Bian, Z., Gu, Y., Zhao, J., Pan, Y. E., Li, Y., Zeng, C. and Wang, L.: Simulation of evapotranspiration based on leaf area index, precipitation and pan evaporation: A case study of Poyang lake watershed, China, Ecohydrol. Hydrobiol., 19, 83–92, https://doi.org/10.1016/j.ecohyd.2018.03.005, 2019.

Xinjiang Uygur Autonomous Region Bureau of Statistics: Xinjiang Statistical Yearbook 2015, https://tjj.xinjiang.gov.cn/ (last access: 17 June 2026), 2016.

Campbell, B. M., Beare, D. J., Bennett, E. M., Hall-Spencer, J. M., Ingram, J. S. I., Jaramillo, F., Ortiz, R., Ramankutty, N., Sayer, J. A., and Shindell, D.: Agriculture production as a major driver of the Earth system exceeding planetary boundaries, Ecol. Soc., 22, 8, https://doi.org/10.5751/ES-09595-220408, 2017.

Cao, Z., Zhu, T., and Cai, X.: Hydro-agro-economic optimization for irrigated farming in an arid region: the Hetao Irrigation District, Inner Mongolia, Agric. Water Manage., 277, 108095, https://doi.org/10.1016/j.agwat.2022.108095, 2023.

Chen, D., Zeng, X., Gui, D., Wang, D., and Wu, J.: Quantifying the hydrological processes in the Tarim River Basin, China, using a coupled groundwater/surface water model, Hydrogeol. J., 33, 1637–1661, https://doi.org/10.1007/s10040-025-02947-7, 2025.

Chen, S.: Optimal allocation of water resources in the Tarim River mainstream based on "three red lines", Master thesis, Huazhong University of Science and Technology, https://doi.org/10.27157/d.cnki.ghzku.2019.003542, 2019.

Chen, Y.-N., Zilliacus, H., Li, W.-H., Zhang, H.-F., and Chen, Y.-P.: Ground-water level affects plant species diversity along the lower reaches of the Tarim river, Western China, J. Arid Environ., 66, 231–246, https://doi.org/10.1016/j.jaridenv.2005.11.009, 2006.

Copernicus Climate Change Service (C3S): ERA5-Land hourly data from 1950 to present, Copernicus Climate Change Service (C3S) Climate Data Store (CDS [data set],) https://doi.org/10.24381/cds.e2161bac, 2019.

Cosgrove, W. J. and Loucks, D. P.: Water management: current and future challenges and research directions, Water Resour. Res., 51, 4823–4839, https://doi.org/10.1002/2014WR016869, 2015.

CSR (Center for Space Research): GRACE terrestrial water storage anomalies, University of Texas at Austin [data set], https://doi.org/10.5067/TEMSC-3JC63, 2023.

Cui, B., Wang, G., Wei, G., Gui, D., Abd-Elmabod, S. K., Goethals, P., and Ahmed, Z.: Proactive policies are the key to reversing desertification in the main stream of the Tarim River in the past 30 years, J. Environ. Manage., 370, 122919, https://doi.org/10.1016/j.jenvman.2024.122919, 2024.

Deb, K. and Jain, H.: An Evolutionary Many-Objective Optimization Algorithm Using Reference-Point-Based Nondominated Sorting Approach, Part I: Solving Problems With Box Constraints, IEEE T. Evol. Comput., 18, 577–601, https://doi.org/10.1109/TEVC.2013.2281535, 2014.

Dou, X., Ma, X., Huo, T., Zhu, J., and Zhao, C.: Assessment of the environmental effects of ecological water conveyance over 31 years for a terminal lake in Central Asia, CATENA, 208, 105725, https://doi.org/10.1016/j.catena.2021.105725, 2022.

FAO: Coping with water scarcity: an action framework for agriculture and food security. FAO Water Reports No. 38, Food and Agriculture Organization of the United Nations, Rome, Italy, ISBN 978-92-5-107304-9, 2012.

Feng, M., Chen, Y., Duan, W., Fang, G., Li, Z., Jiao, L., Sun, F., Li, Y., and Hou, Y.: Comprehensive evaluation of the water-energy-food nexus in the agricultural management of the Tarim River Basin, Northwest China, Agr. Water Manage., 271, 107811, https://doi.org/10.1016/j.agwat.2022.107811, 2022.

Flörke, M., Schneider, C., and McDonald, R. I.: Water competition between cities and agriculture driven by climate change and urban growth, Nat. Sustain., 1, 51–58, https://doi.org/10.1038/s41893-017-0006-8, 2018.

Gao, B., Xu, J., Deng, M., and Ling, H.: Study on the synergistic effects of ecological water conveyance and climate change on ecological restoration in arid areas: A case study of the Tarim River Basin, Ecol. Eng., 222, 107793, https://doi.org/10.1016/j.ecoleng.2025.107793, 2026.

Gong, P., Wang, J., Yu, L., Zhao, Y., Liang, L., Niu, Z., Huang, X., Fu, H., Liu, S., Li, C., Li, X., Fu, W., Liu, C., Xu, Y., Wang, X., Cheng, Q., Hu, L., Yao, W., Zhang, H., Zhu, P., Zhao, Z., Zhang, H., Zheng, Y., Ji, L., Zhang, Y., Chen, H., Yan, A., Guo, J., Yu, L., Wang, L., Liu, X., Shi, T., Zhu, M., Chen, Y., Yang, G., Tang, P., Xu, B., Giri, C., Clinton, N., Zhu, Z., Chen, J., and Chen, J.: Finer resolution observation and monitoring of global land cover: first mapping results with Landsat TM and ETM+ data, Int. J. Remote Sens., 34, 2607–2654, https://doi.org/10.1080/01431161.2012.748992, 2013.

Grashey-Jansen, S., Kuba, M., Cyffka, B., Halik, Ü., and Aishan, T.: Spatio-temporal Variability of Soil Water at Three Seasonal Floodplain Sites: A Case Study in Tarim Basin, Northwest China, Chinese Geogr. Sci., 24, 647–657, https://doi.org/10.1007/s11769-014-0717-y, 2014.

Hao, Z., Chen, S., Li, Z., Yu, Z., Shao, Q., Yuan, F., and Shi, F.: Quantitative assessment of the impacts of irrigation on surface water fluxes in the Tarim River, China, Hydrol. Res., 46, 996–1007, https://doi.org/10.2166/nh.2015.215, 2015.

Hartmann, H., Snow, J. A., Su, B., and Jiang, T.: Seasonal predictions of precipitation in the Aksu-Tarim River basin for improved water resources management, Global Planet. Change, 147, 86–96, https://doi.org/10.1016/j.gloplacha.2016.10.018, 2016.

Hersbach, H., Bell, B., Berrisford, P., Hirahara, S., Horányi, A., Muñoz-Sabater, J., Nicolas, J., Peubey, C., Radu, R., Schepers, D., Simmons, A., Soci, C., Abdalla, S., Abellan, X., Balsamo, G., Bechtold, P., Biavati, G., Bidlot, J., Bonavita, M., De Chiara,

G., Dahlgren, P., Dee, D., Diamantakis, M., Dragani, R., Flemming, J., Forbes, R., Fuentes, M., Geer, A., Haimberger, L., Healy, S., Hogan, R. J., Hólm, E., Janisková, M., Keeley, S., Laloyaux, P., Lopez, P., Lupu, C., Radnoti, G., de Rosnay, P., Rozum, I., Vamborg, F., Villaume, S., and Thépaut, J.-N.: The ERA5 global reanalysis, Q. J. R. Meteorol. Soc., 146, 1999–2049, https://doi.org/10.1002/qj.3803, 2020.

Hou, X.: 1 : 1 million vegetation map of China, National Tibetan Plateau / Third Pole Environment Data Center [data set], http://data.tpdc.ac.cn (last access: 17 June 2026), 2019.

IPCC: Summary for policymakers, in: Climate Change 2022: Impacts, Adaptation and Vulnerability, Cambridge University Press, https://doi.org/10.1017/9781009157940.001, 2022.

Jalilov, S., Amer, S. A., and Ward, F. A.: Managing the water-energy-food nexus: opportunities in Central Asia, J. Hydrol., 557, 407–425, https://doi.org/10.1016/j.jhydrol.2017.12.040, 2018.

Jia, Z.: Research on optimal allocation of ecological water in the main stream of Tarim, MS thesis, Huazhong University of Science and Technology, Wuhan, China, https://doi.org/10.27157/d.cnki.ghzku.2020.005646, 2020.

Jiang, L., Chen, X., and Bao, A.: Analysis on the Changing Dynamics of Groundwater Level in the Lower Reaches of the Tarim River, Xinjiang, Arid Land Geogr., 28, 33–37, https://doi.org/10.13826/j.cnki.cn65-1103/x.2005.01.007, 2005. (In Chinese)

Jiao, A., Wang, W., Ling, H., Deng, X., Yan, J., and Chen, F.: Effect evaluation of ecological water conveyance in Tarim River Basin, China, Front. Environ. Sci., 10, 1019695, https://doi.org/10.3389/fenvs.2022.1019695, 2022.

Karner, K., Schmid, E., Schneider, U. A., and Mitter, H.: Computing stochastic Pareto frontiers between economic and environmental goals for a semi-arid agricultural production region in Austria, Ecol. Econ., 185, 107044, https://doi.org/10.1016/j.ecolecon.2021.107044, 2021.

Li, H., Zhang, Y., Chiew, F. H., and Xu, S.: Predicting runoff in ungauged catchments by using Xinanjiang model with MODIS leaf area index, J. Hydrol., 370, 155–162, https://doi.org/10.1016/j.jhydrol.2009.03.003, 2009.

Li, W., Hao, A., Liu, Z., and Wan, L. Research on Prospective Areas for Groundwater Exploration in the Tarim Basin, Beijing: Geological Publishing House, 149 pp., ISBN 7-116-03169-3, 2003 (in Chinese).

Li, Z., Wang, Y., Chang, J., Guo, A., Wang, L., Niu, C., Hu, R., and He, B.: Multi-objective double layer water optimal allocation and scheduling framework combing the integrated surface water – groundwater model, Water Res., 262, 122141, https://doi.org/10.1016/j.watres.2024.122141, 2024.

Liao, L., Xue, Z., Dong, B., Zhu, K., Zhang, Q., Wei, F., Fu, G., and Wei, G.: Cumulative Ecohydrological Response to Hydrological Processes in Arid Basins, Ecol. Indic., 111, 106005, https://doi.org/10.1016/j.ecolind.2019.106005, 2020.

Ling, H., Guo, B., Xu, H., and Fu, J.: Configuration of water resources for a typical river basin in an arid region of China based on the ecological water requirements (EWRs) of desert riparian vegetation, Global Planet. Change, 122, 292–304, https://doi.org/10.1016/j.gloplacha.2014.09.008, 2014.

Lu, C., Feng, Q., Gao, X., Liu, W., and Ning, T.: Human–water adaptation in drylands: Reconciling water use and ecological security in arid inland river basins of China, J. Clean. Prod., 542, 147561, https://doi.org/10.1016/j.jclepro.2026.147561, 2026.

Markstrom, S. L., Niswonger, R. G., Regan, R. S., Prudic, D. E., and Barlow, P. M.: GSFLOW – Coupled Ground-Water and Surface-Water Flow Model Based on the Integration of the Precipitation-Runoff Modeling System (PRMS) and the Modular Ground-Water Flow Model (MODFLOW-2005), U.S. Geological Survey Techniques and Methods, Book 6, Chap. D1, 240 pp., https://doi.org/10.3133/tm6D1, 2008.

Martens, B., Miralles, D. G., Lievens, H., van der Schalie, R., de Jeu, R. A. M., Fernández-Prieto, D., Beck, H. E., Dorigo, W. A., and Verhoest, N. E. C.: GLEAM v3: satellite-based land evaporation and root-zone soil moisture, Geosci. Model Dev., 10, 1903–1925, https://doi.org/10.5194/gmd-10-1903-2017, 2017.

Meng, X., Mao, K., Meng, F., Shi, J., Zeng, J., Shen, X., Cui, Y., Jiang, L., and Guo, Z.: A fine-resolution soil moisture dataset for China in 2002–2018 (3.0). Zenodo [data set], https://doi.org/10.5281/zenodo.4738556, 2021a.

Meng, X., Mao, K., Meng, F., Shi, J., Zeng, J., Shen, X., Cui, Y., Jiang, L., and Guo, Z.: A fine-resolution soil moisture dataset for China in 2002–2018, Earth Syst. Sci. Data, 13, 3239–3261, https://doi.org/10.5194/essd-13-3239-2021, 2021.

Ministry of Agriculture and Rural Affairs of Xinjiang: National Agricultural Product Cost-Benefit Compilation and Annual Crop Price Statistics. Urumqi: Ministry of Agriculture and Rural Affairs of Xinjiang, https://nynct.xinjiang.gov.cn/ (last access: 19 June 2026), 2025.

Miralles, D. G., De Jeu, R. A. M., Gash, J. H., Holmes, T. R. H., and Dolman, A. J.: Magnitude and variability of land evaporation and its components at the global scale, Hydrol. Earth Syst. Sci., 15, 967–981, https://doi.org/10.5194/hess-15-967-2011, 2011.

Naranjo, L., Correa-Cano, M. E., Rey, D., Chengot, R., España, F., Sactic, M., Knox, J. W., Yan, X., Viteri-Salazar, O., Foster, W., and Melo, O.: A scenario-specific nexus modelling toolkit to identify trade-offs in the promotion of sustainable irrigated agriculture in Ecuador, a Belt and Road country, J. Clean. Prod., 413, 137350, https://doi.org/10.1016/j.jclepro.2023.137350, 2023.

NASA/METI/AIST/Japan Spacesystems and U.S./Japan ASTER Science Team: ASTER Global Digital Elevation Model Version 3 (ASTGTM V003), NASA EOSDIS Land Processes Distributed Active Archive Center, https://doi.org/10.5067/ASTER/ASTGTM.003, 2019.

National Bureau of Statistics of China: China Statistical Yearbook (2002–2021), https://www.stats.gov.cn/ (last access: 17 June 2026), 2021.

Niu, G., Zheng, Y., Han, F., and Qin, H.: The nexus of water, ecosystems and agriculture in arid areas: a multi-objective optimization study on system efficiencies, Agr. Water Manage., 223, 105697, https://doi.org/10.1016/j.agwat.2019.105697, 2019.

Pang, Z., Huang, T., and Chen, Y.: Diminished groundwater recharge and circulation relative to degrading riparian vegetation in the middle Tarim River, Xinjiang Uygur, Western China, Hydrol. Process., 24, 147–159, https://doi.org/10.1002/hyp.7438, 2010.

Paul, M., Rajib, A., Negahban-Azar, M., Shirmohammadi, A., and Srivastava, P.: Improved agricultural water management in data-scarce semi-arid watersheds: Value of integrating remotely sensed leaf area index in hydro-

logical modeling, Sci. Total Environ., 791, 148177, https://doi.org/10.1016/j.scitotenv.2021.148177, 2021.

Qiu, Y. and Wang, X.: Daily fractional snow cover dataset over High Asia (2002–2018), National Cryosphere Desert Data Center [data set], https://doi.org/10.11922/sciencedb.457, 2020.

Saidmamatov, O., Rudenko, I., Pfister, S., and Koziel, J.: Water-Energy-Food Nexus Framework for Promoting Regional Integration in Central Asia, Water, 12, 1896, https://doi.org/10.3390/w12071896, 2020.

Save, H.: CSR GRACE and GRACE-FO RL06 Mascon Solutions v02, University of Texas at Austin [data set], https://doi.org/10.15781/cgq9-nh24, 2020.

Save, H., Bettadpur, S., and Tapley, B. D.: High resolution CSR GRACE RL05 mascons, J. Geophys. Res.-Sol. Ea., 121, 7547–7569, https://doi.org/10.1002/2016JB013007, 2016.

Song, J., Yang, Y., Sun, X., Lin, J., Wu, M., Wu, J., and Wu, J.: Basin-scale multi-objective simulation-optimization modeling for conjunctive use of surface water and groundwater in northwest China, Hydrol. Earth Syst. Sci., 24, 2323–2341, https://doi.org/10.5194/hess-24-2323-2020, 2020.

Tang, X., Huang, Y., Pan, X., Liu, T., Ling, Y., and Peng, J.: Managing the water-agriculture-environment-energy nexus: trade-offs and synergies in an arid area of Northwest China, Agr. Water Manage., 295, 108776, https://doi.org/10.1016/j.agwat.2024.108776, 2024.

Tao, J., Zuo, Q., Xue, H., Wang, Y., and Zhang, L.: Control indicators and determination method of the "three red lines" in the strictest water resources management system, Water Sav. Irrig., 4, 64–67, https://kns.cnki.net/kcms/detail/detail.aspx?dbcode=CJFD&filename=JSGU201204019 (last access: 17 June 2026), 2012.

Tuoliewubieke, D., Yao, J., Mao, W., Chen, P., Ma, L., Chen, J., and Li, S.: Dominant spring precipitation anomaly modes and circulation characteristics in the Tarim Basin, Central Asia, Atmos. Res., 313, 107767, https://doi.org/10.1016/j.atmosres.2024.107767, 2025.

Wang, G., Xu, S., and Xie, Z.: Study on suitable lake area of Taitema Lake, Groundwater, 41, 6–10, https://doi.org/10.16616/j.cnki.11-4446/TV.2021.09.02, 2021 (in Chinese).

Wang, X., Xu, H., Liu, K., Zhao, X., Wei, G., Aili, A., and Zheng, G.: Ecological water conveyance-driven wetland hydrological connectivity and morphological changes in arid regions: An analysis of the Taitema Lake wetland, J. Environ. Manage., 385, 125615, https://doi.org/10.1016/j.jenvman.2025.125615, 2025.

Wang, Y., Guo, X., Zhang, F., Yin, H., Guo, P., Zhang, W., and Li, Q.: The spatially-distributed ANN-optimization approach for water-agriculture-ecology nexus management under uncertainties and risks, Agr. Water Manage., 271, 107780, https://doi.org/10.1016/j.agwat.2022.107780, 2022.

Watson, J. E. M., Iwamura, T., and Butt, N.: Mapping vulnerability and conservation adaptation strategies under climate change, Nat. Clim. Change, 3, 989–994, https://doi.org/10.1038/nclimate2007, 2013.

Wieder, W. R., Boehnert, J., Bonan, G. B., and Langseth, M.: Harmonized World Soil Database (version 1.2), ORNL DAAC [data set], https://doi.org/10.3334/ORNLDAAC/1247, 2014.

Wu, W., Clark, J. S., and Vose, J. M.: Assimilating multi-source uncertainties of a parsimonious conceptual hydrological model using hierarchical Bayesian modeling, J. Hydrol., 394, 436–446, https://doi.org/10.1016/j.jhydrol.2010.09.017, 2010.

Xinjiang Uygur Autonomous Region Water Resources Department: Xinjiang Water Resources Bulletin (data series, 2002–2021), https://slt.xinjiang.gov.cn/ (last access: 17 June 2026), 2021.

Xu, H., Ye, M., Song, Y., and Chen, Y.: The Natural Vegetation Responses to the Groundwater Change Resulting from Ecological Water Conveyances to the Lower Tarim River, Environ. Monit. Assess., 131, 37–48, https://doi.org/10.1007/s10661-006-9455-7, 2007.

Xue, D., Gui, D., Ci, M., Liu, Q., Wei, G., and Liu, Y.: Spatial and temporal downscaling schemes to reconstruct high-resolution GRACE data: A case study in the Tarim River Basin, Northwest China, Sci. Total Environ., 907, 167908, https://doi.org/10.1016/j.scitotenv.2023.167908, 2024.

Ye, Z., Chen, S., Zhang, Q., Liu, Y., and Zhou, H.: Ecological water demand of Taitema Lake in the lower reaches of the Tarim River and the Cherchen River, Remote Sens., 14, 832, https://doi.org/10.3390/rs14040832, 2022.

Yin, Z., Wu, J., Song, J., Yang, Y., Zhu, X., and Wu, J.: Multi-objective optimization-based reactive nitrogen transport modeling for the water-environment-agriculture nexus in a basin-scale coastal aquifer, Water Res., 212, 118111, https://doi.org/10.1016/j.watres.2022.118111, 2022.

Zafarmomen, N., Alizadeh, H., Bayat, M., Ehtiat, M., and Moradkhani, H.: Assimilation of Sentinel-based leaf area index for modeling surface-ground water interactions in irrigation districts, Water Resour. Res., 60, e2023WR036080, https://doi.org/10.1029/2023WR036080, 2024.

Zeng, X. and Chen, D.: A coupled surface water-groundwater multi-objective optimization framework for coordinated water-ecosystem-agriculture management in arid inland river basin, Zenodo, [data set], https://doi.org/10.5281/zenodo.18151460, 2025.

Zhang, X. and Ren, L.: Simulating and assessing the effects of seasonal fallow schemes on the water-food-energy nexus in a shallow groundwater-fed plain of the Haihe River basin of China, J. Hydrol., 595, 125992, https://doi.org/10.1016/j.jhydrol.2021.125992, 2021.

Zhang, X., Chen, Y., Li, W., Yu, Y., and Sun, Z.: Restoration of the lower reaches of the Tarim River in China, Reg. Environ. Change, 13, 1021–1029, https://doi.org/10.1007/s10113-013-0403-0, 2013.

Zhu, W.: Study on multi-objective water resources allocation scheme in the lower reaches of the Tarim River, Groundwater, 44, 213–215, https://doi.org/10.19807/j.cnki.DXS.2022-02-073, 2022.